Stretchable Seal

Stretchable Seal

Paul Le Floch[1#], Shi Meixuanzi[2#], Jingda Tang[2], Junjie Liu[1, 3], Zhigang Suo[1]*

[1]School of Engineering and Applied Sciences, Kavli Institute for Bionano Science and Technology, Harvard University, MA 02138

[2]State Key Lab for Strength and Vibration of Mechanical Structures, Department of Engineering Mechanics, Xi'an Jiaotong University, Xi'an 710049, China

[3]State Key Laboratory of Fluid Power & Mechatronic System, Key Laboratory of Soft Machines and Smart Devices of Zhejiang Province, and Department of Engineering Mechanics, Zhejiang University, Hangzhou 310027, China

[#]Those authors contributed equally to this work.

*Corresponding author: suo@seas.harvard.edu

KEYWORDS: hermetic seal, stretchable electronics, permeability, wrinkles, laminates

ABSTRACT: Many stretchable electronic devices require stretchable hermetic seals. However, stretchability and permeability are inextricably linked at the molecular level: stretchable, low-permeability materials do not exit. We collect data for permeation of water and oxygen in many materials and describe the scaling relations for both flat and wrinkled seals. Whereas flat seals struggle to fulfill the simultaneous requirements of stretchability, low stiffness and low transmissibility, wrinkled seals can fulfill them readily. We further explore the behavior of wrinkled seals under cyclic stretch using aluminum, polyethylene and silica films on elastomer substrates. The wrinkled aluminum develops fatigue cracks after a small number of cycles, but the wrinkled polyethylene and silica maintain low transmissibility after 10,000 cycles of tensile strain.

INTRODUCTION

Hermetic seals are ubiquitous. Plastics and metals seal food and drug, [1] oxides and nitrides seal microelectronics, [2-3] and butyl rubber seals tires.[4] Except for the last example, seals in general are made of stiff materials: plastics, metals, and ceramics. The recent decade has seen the emergence of stretchable electronics[5-10], soft robots[11-13], hydrogel ionotronics[14], and soft medical devices[15-16]. For long-time use these devices will also require seals. Without hermetic seals, silver nanowires, copper nanowires and liquid metals oxidize[17-19], conducting polymers degarde[20-21], and hydrogels dehydrate[22]. In an island-bridge design of stretchable electronics, non-stretchable electronic materials are placed on stiff islands, which are attached to a soft substrate and are bridged by stretchable interconnects.[23] A stretchable interconnect can be made of a stiff material, by the means of unidirectional buckles, [24-26] or flat serpentines[27-28]. Stiff materials can seal the islands, as well as the buckled and serpentine interconnects, just like a coiled phone cord, which is electrically insulated by a thin layer of plastic. It has been a challenge, however, to seal intrinsically stretchable materials.[29-35] Air-tolerant *and* stretchable functional materials may be developed, such as crumpled graphene[17, 36], but this strategy would push the development of soft devices into a narrow path, excluding many materials of superior electronic properties and well-established processing methods. In general, electronic functions and hermetic seals require different materials.

The search for stretchable seals has highlighted a fundamental fact of nature: stretchable and low-permeability materials do not exist.[22] At the molecular level, stretchability and permeability are inextricably linked. Stretchability comes from the entropic elasticity of polymer chains. In an elastomer, the polymer chains are crosslinked to form a three-dimensional network. To be stretchable, each individual polymer chain contains hundreds or

more monomer units and undergoes ceaseless thermal motion. Consequently, small molecules such as water and oxygen diffuse in an elastomer as readily as in a polymer liquid. The permeability of small molecules in an elastomer is insensitive to crosslink density and applied stretch. An elastomer is solid-like at the scale above the mesh size of the network, but liquid-like at the scale below.

Here we propose to break the stretchability-permeability tradeoff by demonstrating stretchable seals using wrinkled films of stiff materials. We collect data on permeability of water and oxygen for various materials and confirm that no stretchable materials has low enough permeability to serve as hermetic seals for electronics. We develop a scaling model to show that thin and wrinkled films of many stiff materials have both high stretchability and low permeability to serve as stretchable seals. Unlike electrical interconnects made of stiff materials, hermetic seals require two-dimensional, continuous films. To make it stretchable in any in-plane direction, two-dimensional wrinkles are needed. Two-dimensional wrinkles do not affect the permeability of the seal initially, but may develop large local deformation, so that repeated stretch may cause fatigue cracks. To explore these fundamental considerations, we study wrinkled aluminum, polyethylene and silica films on elastomer substrates. We show that the wrinkled the aluminum film develops fatigue cracks after a small number of cycles, but the wrinkled polyethylene and silica films maintain low transmissibility after 10,000 cycles of tensile strain.

a

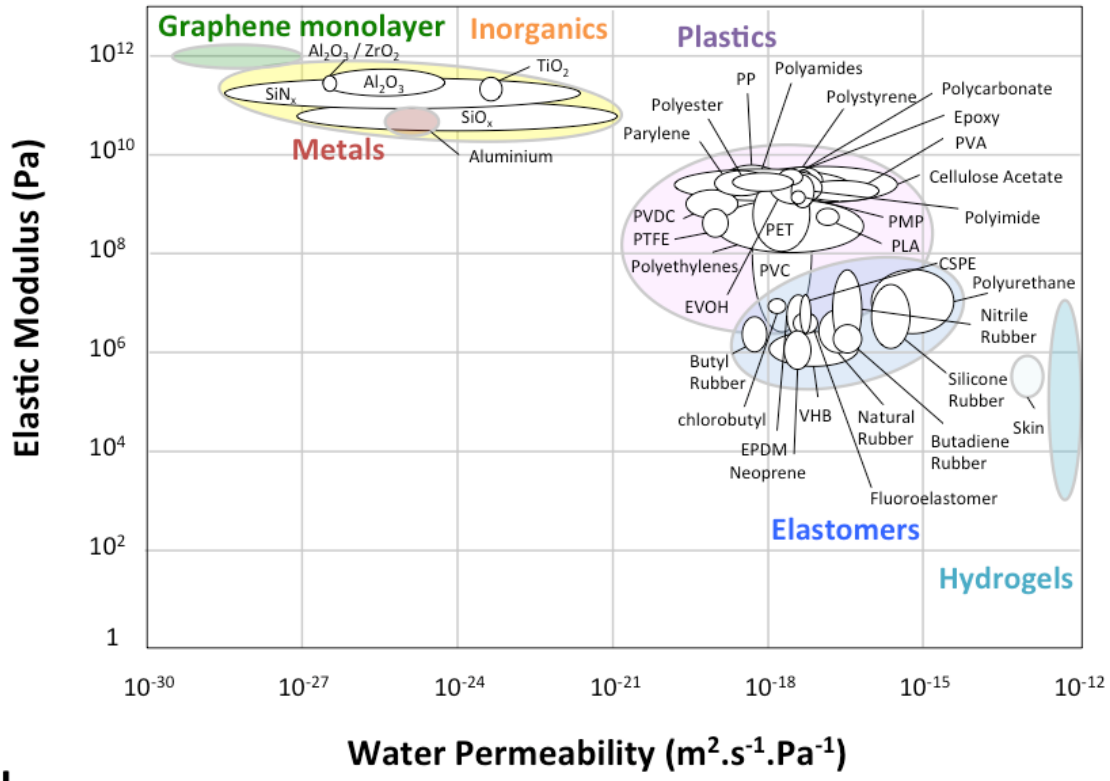
Graphene monolayer
Inorganics
Plastics
Metals
Elastomers
Hydrogels
Elastic Modulus (Pa)
Water Permeability (m².s⁻¹.Pa⁻¹)
Al2O3 / ZrO2
Al2O3
TiO2
SiNx
SiOx
Aluminium
PP
Polyamides
Polystyrene
Polycarbonate
Polyester
Parylene
Epoxy
PVA
Cellulose Acetate
Polyimide
PVDC
PTFE
PET
PMP
PLA
Polyethylenes
PVC
CSPE
Polyurethane
EVOH
Nitrile Rubber
Butyl Rubber
Silicone Rubber
chlorobutyl
VHB
Natural Rubber
Skin
EPDM
Neoprene
Butadiene Rubber
Fluoroelastomer

b

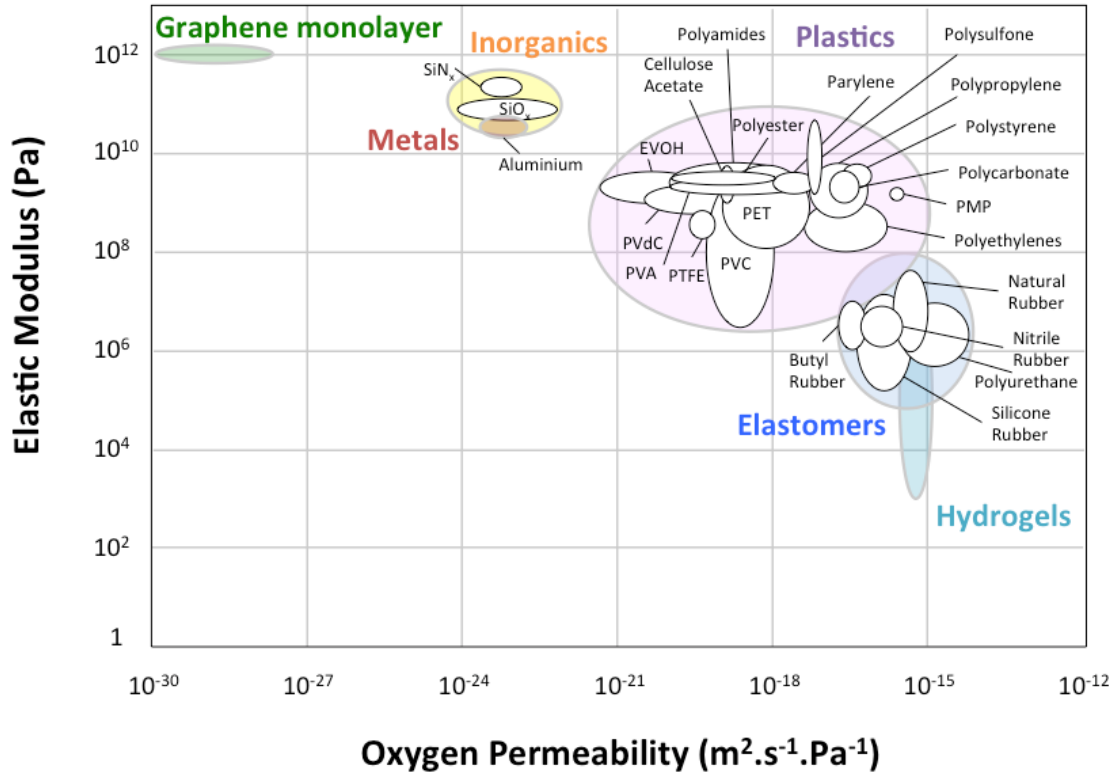
Graphene monolayer
Inorganics
Plastics
Metals
Elastomers
Hydrogels
Elastic Modulus (Pa)
Oxygen Permeability (m².s⁻¹.Pa⁻¹)
SiNx
SiOx
Aluminium
Polyamides
Polysulfone
Cellulose Acetate
Parylene
Polypropylene
Polyester
Polystyrene
EVOH
Polycarbonate
PET
PMP
PVdC
Polyethylenes
PVA
PTFE
PVC
Natural Rubber
Nitrile Rubber
Butyl Rubber
Polyurethane
Silicone Rubber

Figure 1. Soft and low-permeability materials do not exist. Materials are plotted in (a) the space of water permeability and elastic modulus and, (b) the space of oxygen permeability and elastic modulus.

The transmissibility T of a gas through a solid film is defined by[37]

$$\boldsymbol{T = \frac{P}{h} = \frac{J}{\Delta \Pi}} \quad (1)$$

where h (m) is the thickness of the film, P ($m^2.s^{-1}.Pa^{-1}$) is the permeability, $\Delta\prod$ (Pa) is the difference in the partial pressures of the gas on the two sides of the film, and J is the flux of molecules of the gas through the film ($m^3.m^{-2}.s^{-1}$).

We plot various materials in the space of water permeability and elastic modulus, as well as in the space of oxygen permeability and elastic modulus (Figure 1). The data correspond to measurement carried out at ambient pressure and in the temperature range 23 – 40°C. We show in supplementary information that thermal activation of permeability is negligible within this range of temperature compared to the scattering in the data gathered for each material. Also see supplementary information for sources of data and notes on their methods of determination (Table S1) [22, 38-98]. This is perhaps the first time that such a broad range of materials are compared in the permeability-modulus space. Data gathered for each individual material scatter significantly. The permeability of an elastomer or a plastic scatters over one to two orders of magnitude. The permeability of an inorganic material such as silica and silicon nitride scatters even more. This scattering results from two factors. First, the permeability depends on microstructures of materials. For instance, defects in vitreous silica

can affect its permeability. [99-101] Second, permeability is measured under different conditions, such as different temperature or gas pressure (Table S1).

For all the materials gathered here, modulus spans over 10 orders of magnitude, and permeability spans over 15 orders of magnitude. A graphene monolayer has an elastic modulus of 1 TPa and a water-permeability lower than 10^{-27} $m^2.s^{-1}.Pa^{-1}$. For conventional electronic packaging[2], the inorganic materials such as silicon dioxide and silicon nitride are used. These passivation layers suffer from pinholes and cracks. Organic sealants like epoxies, polyimide, and polyxyxylene (Parylene), are sometimes used instead. For flexible electronics like OLED displays, flexibility of the seal is an additional constraint, and polymer-inorganic multilayered architectures have been developed.[3] Elastomers and hydrogels have low elastic modulus but high permeability. The large white holes in both spaces affirm the fundamental fact of nature: soft and low-permeability materials do not exist.

Of all materials, only elastomers are capable of large and elastic stretch. Among elastomers, the butyl rubber is the least permeable, but its permeability for water and oxygen is more than 10,000 times that of silicon dioxide (Figure 1).[22, 47-51, 87, 102] Butyl rubber has been proposed to seal flexible and stretchable electronics,[102-103] but its efficacy is uncertain. The information on water and oxygen sensitivity for stretchable electronic materials is scanty and mostly qualitative. In microelectronics, it is common practice to seal devices with a silicon dioxide layer of at least 100 nm. According to equation (1), however, 1 mm of butyl rubber must be used to reach the same level of transmissibility. As another example, to last more than 10,000 hours, OLEDs and organic solar cells[3, 98, 104-105] require a water vapor transmission rate (WVTR) lower than 10^{-6} $g/m^2/day$ (i.e., a transmissibility of 8×10^{-21} m/s/Pa), and an oxygen transmission rate (OTR) lower than 10^{-5} $mL/m^2/day$ (i.e., a transmissibility of 6×10^{-21} m/s/Pa),

assuming that the relative humidity difference is 50% and that the oxygen partial pressure is 21 kPa in the ambient atmosphere. A thickness of 0.5 to 5 millimeters would be required to satisfy the WVTR criteria, and a thickness of about 10 centimeters is required to satisfy the OTR criteria. Again, a butyl rubber seal would be even thicker than submillimeter devices.

Composites have long been used as seals in the food packaging industry, as well as the OLED coating industry. A stiff, low-permeability material (e.g., an oxide, a nitride, or graphene) is integrated as barriers in a matrix (e.g., a plastic or an elastomer).[106-108] The barrier material can be used as a continuous layer, or as nanoparticles with a large aspect ratio. The former is the laminate structure, and the latter is the brick-mortar structure. Both structures can lower the permeation of small molecules, but neither can be made soft and stretchable (Figure S1, S2).

STIFFNESS–TRANSMISSIBILITY TRADEOFF

For a seal of permeability P and thickness h, the transmissibility is $T = P/h$. When a flat film is stretched, the stiffness is Eh, where E is the elastic modulus. When a wrinkled film is stretched, the stiffness scales as Eh^3/L^2, where L is the period of the wrinkles. The trade-off between stiffness and transmissibility is different for a flat and a wrinkled seal. These relations and their implications for stretchable seals are discussed in this section. For numerical illustration, we will use water permeability for various materials.

Stiffness of a flat seal. Consider a flat seal under uniaxial tension (Figure 2). The force F is proportional to the tensile strain $\delta l/l$:

$$\frac{F}{w} = Eh\frac{\delta l}{l}, \qquad (2)$$

where w is the width of the film, and Eh, the stiffness. We plot each material as a parallelogram in the space of stiffness and transmissibility (Figure 2). The top edge of a parallelogram corresponds to the stiffness of a material of a thickness of 1 mm, and the bottom edge corresponds to a thickness of 10 nm. The horizontal width of the parallelogram corresponds to the scatter in the permeability of the material (Table S1). As a numerical illustration, we draw a vertical line corresponding to the required limit of transmissibility for OLEDs previously mentioned.[3] The seal needs to limit the transmissibility to the left of the vertical line. All plastics and elastomers are too permeable to fulfill the requirement. All the stiff seals can be used to protect flexible electronics provided the strain of the devices is sufficiently small to avoid breaking.[109] Graphene and ultrathin films of oxides and nitrides may sustain a few percent of tensile strain.[81, 110-111] They may potentially be used to seal devices of small stretchability. We draw a horizontal line corresponding to a soft device of a modulus of 1 MPa and a thickness of 1 mm, which gives a stiffness of 10^3 $N.m^{-1}$. We stipulate that the stiffness of the seal should not exceed that of the device, which limits the stiffness of the seal below the horizontal line. The lower left quadrant of the stiffness-transmissibility is empty. A 100 nm-thick silica seal is too stiff, but stays within the required limit of transmissibility. According to the lowest value of transmissibility reported in the literature[80], a graphene monolayer (0.335 nm thick, indicated by the horizontal green segment in Figure 2) is compliant enough, and approximately fulfills the transmissibility criteria.

In the above, we have drawn the vertical and horizontal lines under certain assumptions. Under different assumptions, the two lines will move, and the lower left quadrant may contain some candidates. However, it will be a challenge for flat seals to have both low stiffness and low transmissibility.

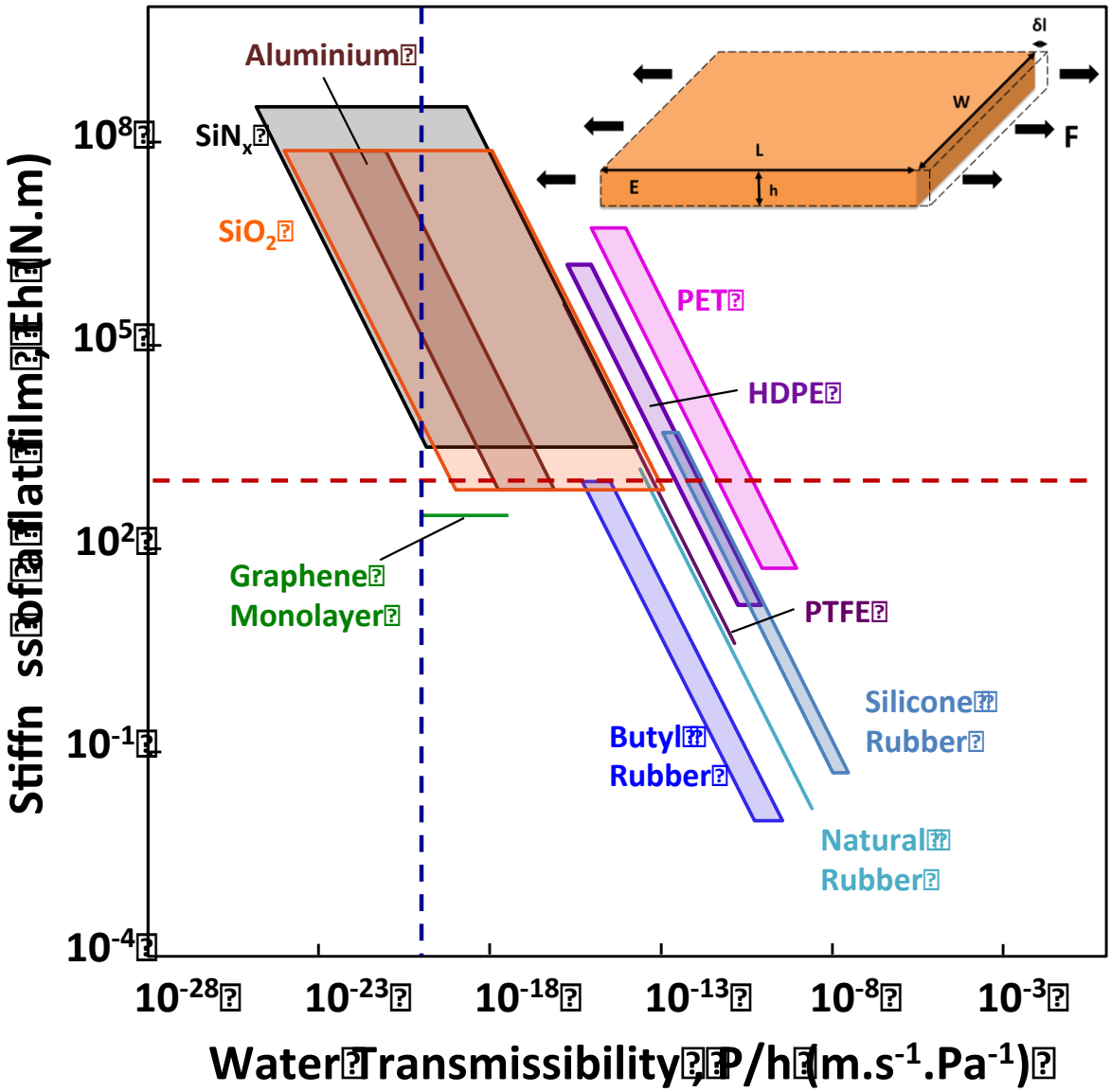

Figure 2. Stiffness-transmissibility diagram for flat seals. Each material is represented by a parallelogram, where the water permeability varies between a maximum and a minimum value (according to Table S1) and the thickness h varies between 1 mm and 10 nm.

Stiffness of a wrinkled seal. We consider now a seal with a wavy shape in one direction, attached to a substrate (i.e. a soft device) at the troughs of the wave (Figure 3). When an in-plane force F is applied, the seal will be deformed between each attachment point. For an inextensible thin film, the deformation is pure bending. By analogy with the buckling of an

elastica,[112-116] we derived that the force F needed to compress a wrinkled film is (Supplementary Information):

$$\frac{F-F_b}{w} = \frac{5.56}{12(1-\nu)} \frac{Eh^3}{L^2} \frac{\delta L}{L} \quad (5)$$

Where F_b is the force required to initially buckle the film between two attachment points, w and h are respectively the width and the thickness of the film, ν is the Poisson's ratio and E is the elastic modulus of the material, and L is the period of the wrinkles. $\delta L/L$ is the relative change of the wrinkles period. The numerical pre-factor $\frac{5.56}{12(1-\nu)}$ is close to 1. Equation (5) is a linear interpolation for $\delta L/L$ in the range [0 ; 0.2]. This approach shows that the rigidity Eh^3/L^2 is the parameter of interested to describe the stiffness of a wrinkled thin film. This conclusion can also be reached using dimensional analysis (Supplementary Information). The wrinkles stiffness is lower than the stiffness of the flat film by a factor h^2/L^2, and allows large stretchability of the film.

For a wrinkled film, the thickness h is much smaller than the wavelength L. For numerical illustration, we set $h/L = 0.1$, so that $Eh^3/L^2 = 0.01Eh$. We plot each material as a parallelogram in the space of transmissibility and stiffness of a wrinkled film (Figure 3). In this case, the lower left quadrant contains commonly used sealing materials. A 100 nm-thick wrinkled silica seal will fulfill both the transmissibility and the stiffness requirement. Furthermore, the relative change of the wrinkles period, $\delta L/L$, can be large, even though the local deformation is small. As another example, a 100 μm-thick polytetrafluoroethylene (PTFE) can be used to achieve the desired stiffness, but with a transmissibility as low as 10^{-16} $m.s^{-1}.Pa^{-1}$. Here we only considered the case where $h/L = 0.1$, but wrinkles with a larger wavelength could be designed to achieve lower levels of stiffness.

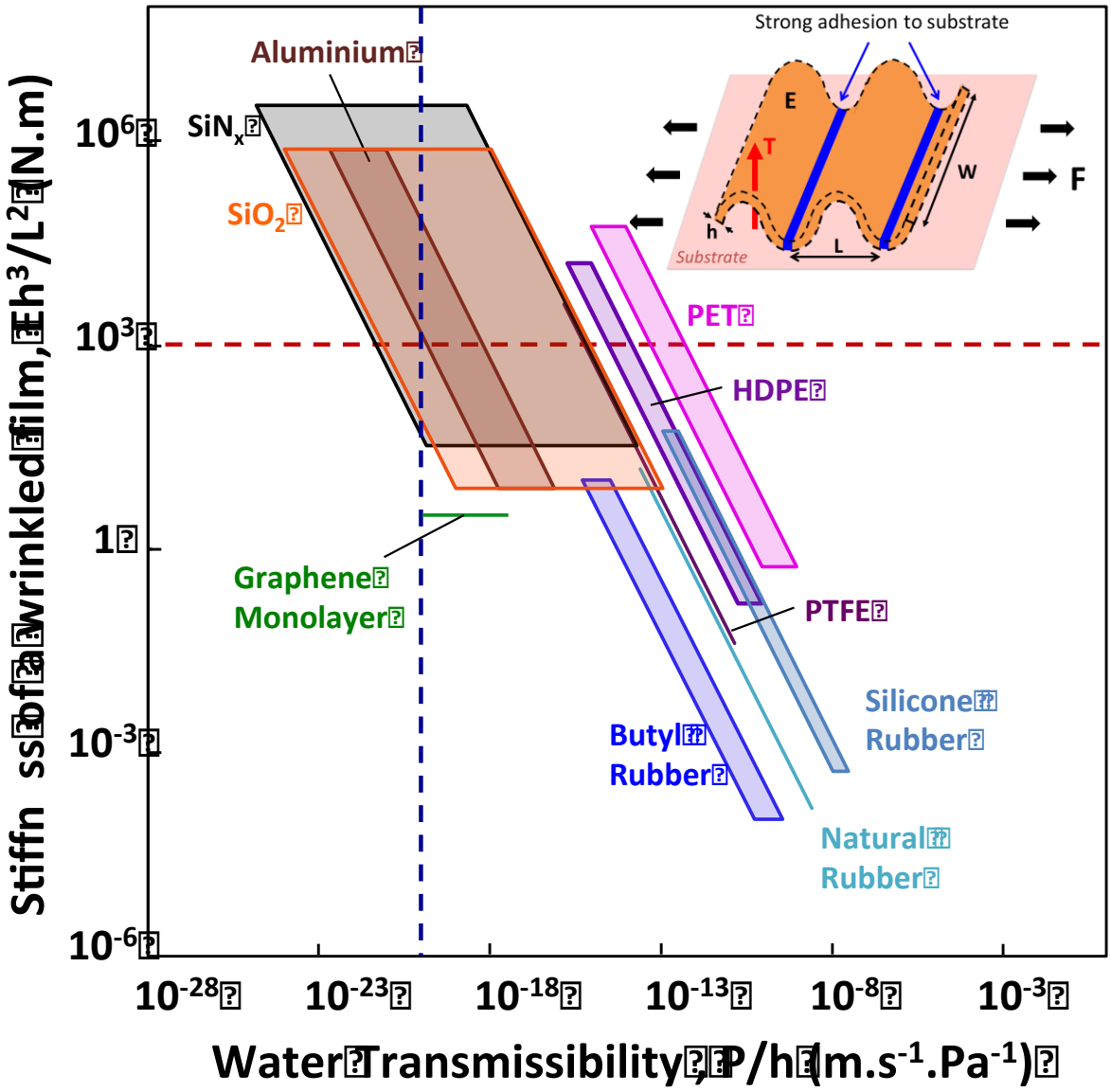

Figure 3. Stiffness-transmissibility diagram for wrinkled seals. Each material is represented by a parallelogram where the water permeability varies between a maximum and a minimum value (according to Table S1) and the thickness *h* varies between 1 mm and 10 nm. For the stiffness of the wrinkled film, we set h/L = 0.1. Thin films of low-permeability materials (e.g., graphene, silica, silicon nitride) give sufficiently low stiffness and low transmissibility.

USING WRINKLES TO MAKE SOFT, LOW-PERMEABILITY SEALS

To illustrate the previous analysis, we prepared wrinkled seals using buckle-delamination[117-118] of a thin, stiff, and low-permeability material on a soft substrate (Figure 4). Uniaxial and biaxial wrinkles were studied. The amount of delamination depends on the substrate – film adhesion, which we did not investigate here. When a film is bent, the strain is given by $\varepsilon = y/R$, where R is the radius of curvature, and y is the distance of material particle in the film from the neutral surface. Using $y \sim h$ and $R \sim L$, we estimate $\varepsilon \sim h/L$. The failure strain is on the order of 1% for stiff materials. These elementary considerations suggest that one should be careful in designing a wrinkled film to avoid rupture. Furthermore, two-dimensional wrinkles may develop localized large deformation. It is difficult to quantify the failure conditions analytically. We use uniaxial tension to study experimentally the stress-stretch behavior and the fatigue of wrinkled seals.

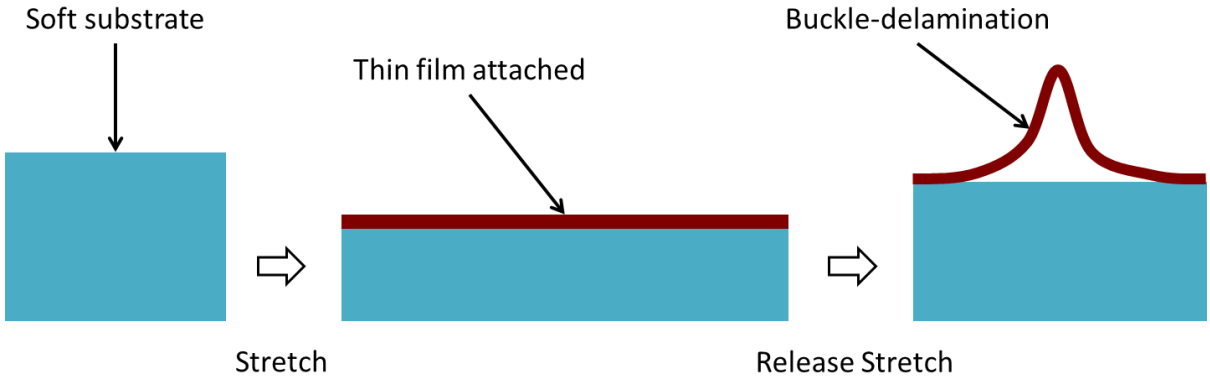

Figure 4. A substrate is pre-stretched, on which a thin film of low-permeability material is attached. When the pre-stretch is released, the film undergoes buckle-delamination.

We studied three film/substrate systems. The first two systems used an acrylic elastomer VHB as the substrate, and a polyethylene and an aluminum foil as the films. As discussed above, polyethylene and aluminum are too permeable to seal air-sensitive devices, but these materials are readily available and easily handled. Here we used them to explore the

behavior of wrinkled seals under cyclic stretch. The third system involves silica films deposited on a polydimethylsiloxane (PDMS) substrate.

For the polyethylene/VHB system, the VHB layer was 500±10 microns thick, the polyethylene film was 27±2 microns thick. We applied both uniaxial and biaxial stretches to the VHB elastomer before attaching polyethylene films. Then the pre-stretch is released and the thin films wrinkle. Figure 5a shows optical micrographs of polyethylene thin film (Glad Press'n Seal food wrap) on a sheet of biaxially pre-stretched VHB (biaxial stretch=2.5x2.5 times). The pre-stretch is then released in both directions simultaneously. After release, the residual stretch is 1.75x1.75. We can clearly see the wrinkles and the delamination in the polyethylene films. The wrinkles have some common features with the herringbone patterns, but are more random.[119-120] Figure 5b shows a polyethylene thin film on a sheet of uniaxially pre-stretched VHB (stretch=4 times). After release, the residual stretch is 1.67.

Similarly, Figure 5c, d show optical micrographs of both biaxial and uniaxial aluminum wrinkles sandwiched between two VHB layers. (Two pre-stretched layers were necessary to induce the buckling instability). The aluminum layer is 26.5±2.4 microns thick, and the VHB layers are 1 or 2 mm thick, depending on the pre-stretch applied. Delamination is much less pronounced for the VHB/aluminum/VHB laminates, but it tends to become more severe as the pre-stretch increases.

Furthermore, we deposited silica films onto polydimethylsiloxane (PDMS), by PECVD (see Materials section for details on the deposition process). Figure 5e, f show respectively SEM and optical images of biaxial and uniaxial silica wrinkles on PDMS. Silica films between 5 and 50 (±0.2) nm were deposited on a pre-stretched (up to 1.30x1.30 times) PDMS substrate (200±10 μm). The residual stretch is negligible for silica wrinkles on PDMS, and we did not observe delamination.

The presence of a residual stretch in some cases can be qualitatively explained by estimating the stiffness of the substrate (Eh) and the wrinkled thin film (Eh^3/L^2). In case of polyethylene/VHB, the substrate has a stiffness in the order of $9x10^2$ N.m. The uniaxial wrinkles period is about 250 μm. Thus, the stiffness of the polyethylene film is about $3x10^2$ N.m. This rough estimation shows that the two stiffnesses are comparable. The wrinkles can thus limit the release of the pre-stretch. In case of silica/PDMS, the substrate has a stiffness in the order of 10^3 N.m. The period of the uniaxial wrinkles is about 6 μm. Thus, the stiffness of the silica film is about $3x10^{-1}$ N.m. The silica wrinkles are much softer than the substrate, which explains why the pre-stretched is completely released.

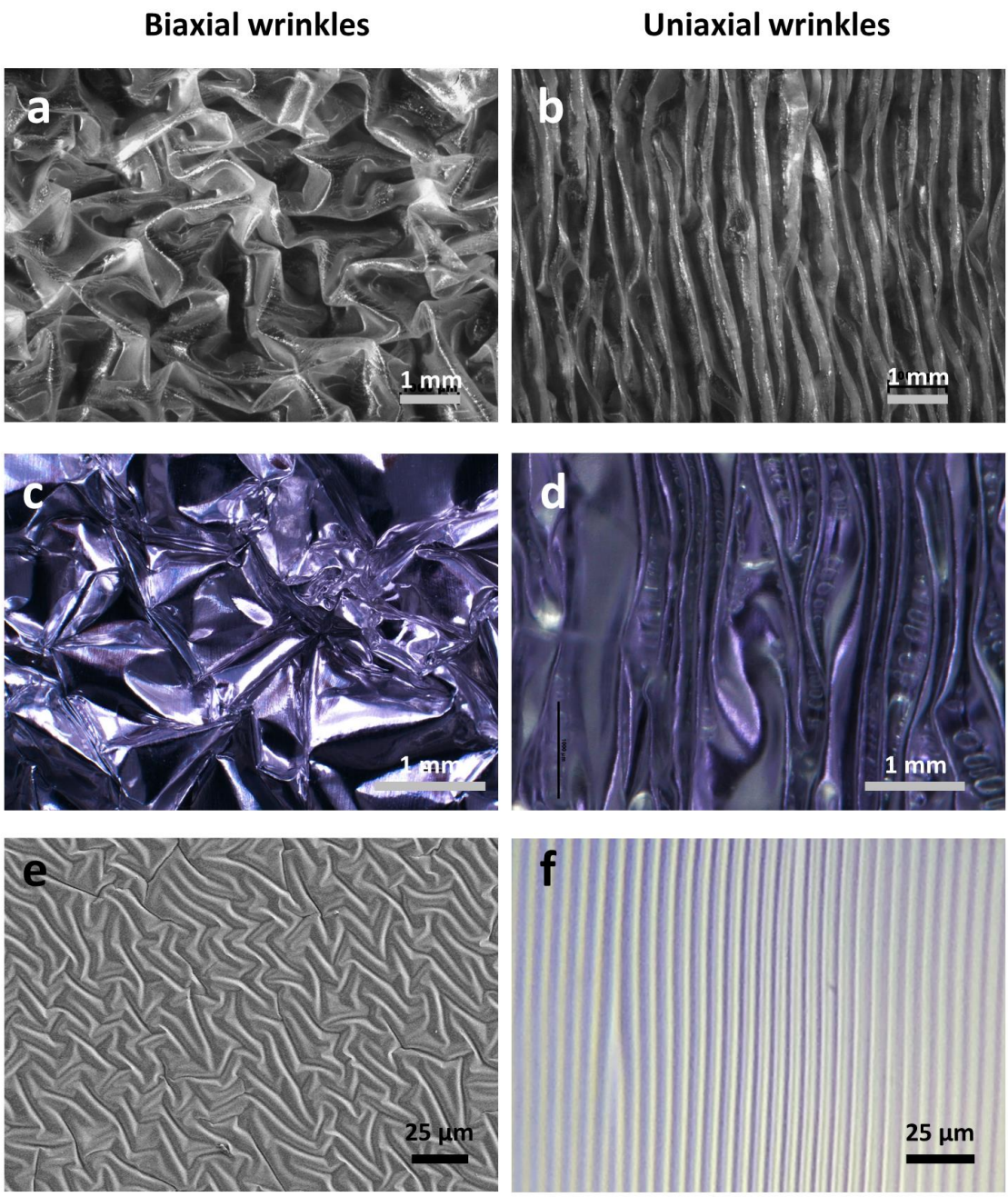

Figure 5. Biaxial and uniaxial wrinkles of various stiff materials on soft substrates. a, Polyethyelene (27 µm) on a biaxially pre-stretched (2.5x2.5 times) VHB (500 µm). After release, the residual biaxial stretch is 1.75x1.75. **b,** Polyethylene on a uniaxially pre-stretched VHB (4 times). After release, the residual uniaxial stretch is 1.67**.** For a and b, scale bars are 1 mm. **c,** Biaxially pre-stretched (4x4 times) VHB (1 mm)/aluminum (26.5 µm)/VHB (1 mm). Scale bar = 5 mm. **d,** Uniaxially pre-stretched (5 times) VHB (2 mm)/aluminum (26.5

μm)/VHB (2 mm). Scale bar =1 mm. **e**, Silica (50 nm) on a biaxially pre-stretched (1.23x1.23 times) PDMS substrate (200 μm). **f**, Silica (50 nm) on a uniaxially pre-stretched (1.20 times) PDMS substrate (200 μm). For e and f, scale bars are 25 μm. The residual stretch is negligible for silica wrinkles on PDMS.

Mechanical properties of the wrinkled laminate. As expected, the laminate of a wrinkled film on an elastomer is stretchable. We use uniaxial tension to quantify the stretchability of uniaxially pre-stretched wrinkled laminates (Figure S5). When the pre-stretch increases, the amplitude of the wrinkles becomes larger, and their wavelength decreases slightly, which leads to a larger stretchability. In uniaxial tension, if the stretch applied is lower than the initial pre-stretch, the wrinkled laminate is stretchable, and almost as soft as the substrate. Stretching further will cause delamination of the coating or cracks. Both scenarios lead to failure of the laminate.

We measured the electrical resistance of the aluminum film while subject the laminate to cyclic stretch (Figure S6a). After a small number of cycles, the resistance of the aluminum jumps to a very high value (Figure S6b), because cracks have propagated through the width of the sample (Figure S6c,d), and the aluminum film is not continuous anymore. Thus, the VHB/aluminum/VHB laminate is not a good choice for designing stretchable seals. By contrast, the polyethylene/VHB and silica/PDMS systems doe not develop cracks under cyclic stretch.

Water Transmissibility of wrinkled laminates. We measured the water transmissibility of polyethylene/VHB and silica/PDMS using the dry cup test[22]. Both laminates have lower water transmissibility than the bare substrates (Figure 6). Wrinkled laminates have a higher water transmissibility than the flat one. It can be explained partially because of the area pre-

stretch and the residual area stretch. Because the elastomer substrate is incompressible, the residual area stretch implies a decrease in thickness (Figure S7), which increases the water transmissibility through the elastomer, according to equation (1). Also, the wrinkled plastic layer has a larger surface than the elastomer substrate (Figure S7). We propose a simple model to consider these effects (Supporting Information), and derive a formula to predict the transmissibility of wrinkled laminates:

$$\frac{1}{T_{eff}} = \frac{1}{\lambda_r}\frac{1}{T_s} + \frac{{\lambda_r}^2}{\lambda_p}\frac{1}{T_f} \quad (6)$$

The effective transmissibility T_{eff} depends on the transmissibility of the elastomer substrate T_s, the transmissibility of the plastic film T_f, the area pre-stretch λ_p and the residual area stretch λ_r. We measured individually the water permeability of VHB and polyethylene (PE), while measuring the transmissibility of the laminates (Figure 6a) simultaneously. We obtained P_{VHB} = (4.19±0.58)x10^{-17} $m^2.s^{-1}.Pa^{-1}$ and P_{PE} = (1.17±0.04)x10^{-18} $m^2.s^{-1}.Pa^{-1}$. These values are in good agreement with our previous measurements for VHB[22] and the literature of polyethylene (Table S1). Similarly, we also measured the water permeability of bare PDMS and silica/PDMS laminates (Figure 6b). We obtained P_{PDMS} = (2.42±0.13)x10^{-16} $m^2.s^{-1}.Pa^{-1}$, which is also in good agreement with our previous measurement[22]. Because silica was deposited by PECVD, we were not able to measure the permeability through silica alone. We extrapolate its permeability using a flat PDMS – Silica laminate and equation (6). For a thickness of 5 nm of Silica, we extrapolate P_{Silica} = (6.77±0.14)x10^{-22} $m^2.s^{-1}.Pa^{-1}$. This value is high for bare silica, still in the range of values that we obtained from the literature about silica / plastics laminates (Table S1). We also measured λ_p and λ_r for each sample, which allows us to use equation (6) to predict the effective water transmissibility of wrinkled laminates (Figure 6a, b). For the polyethylene/VHB system, the prediction for the flat laminate is very close to the experimental measurement. For both systems, predictions for wrinkled laminates are

significantly lower than experimental measurements (Figure S8). It may be due to the creation of defects in the thin film during the release of the pre-stretch, or due to the wrinkles geometry, which is more complex than our model. The absolute error bars on the experimental measurements are one standard deviation. The error bars on the predictions represent the standard uncertainty[121], which takes both the standard deviations on the transmissibility measurements of the substrate and the film and the typical error on the measurements of the stretches into account (equation 30 in Supporting Information). Our model predicts that the transmissibility increases with the area pre-stretch. For the polyethylene/VHB system, although the laminate with biaxial wrinkles has a higher transmissibility than the uniaxial and the flat one, it is important to keep in mind that this sample is much thinner because of the effect above-mentioned. In terms of effective permeability, the laminate with biaxial wrinkles is lower than the uniaxial and the flat one. Furthermore, we noticed that the water transmissibility of laminates does not change over a period of a month.

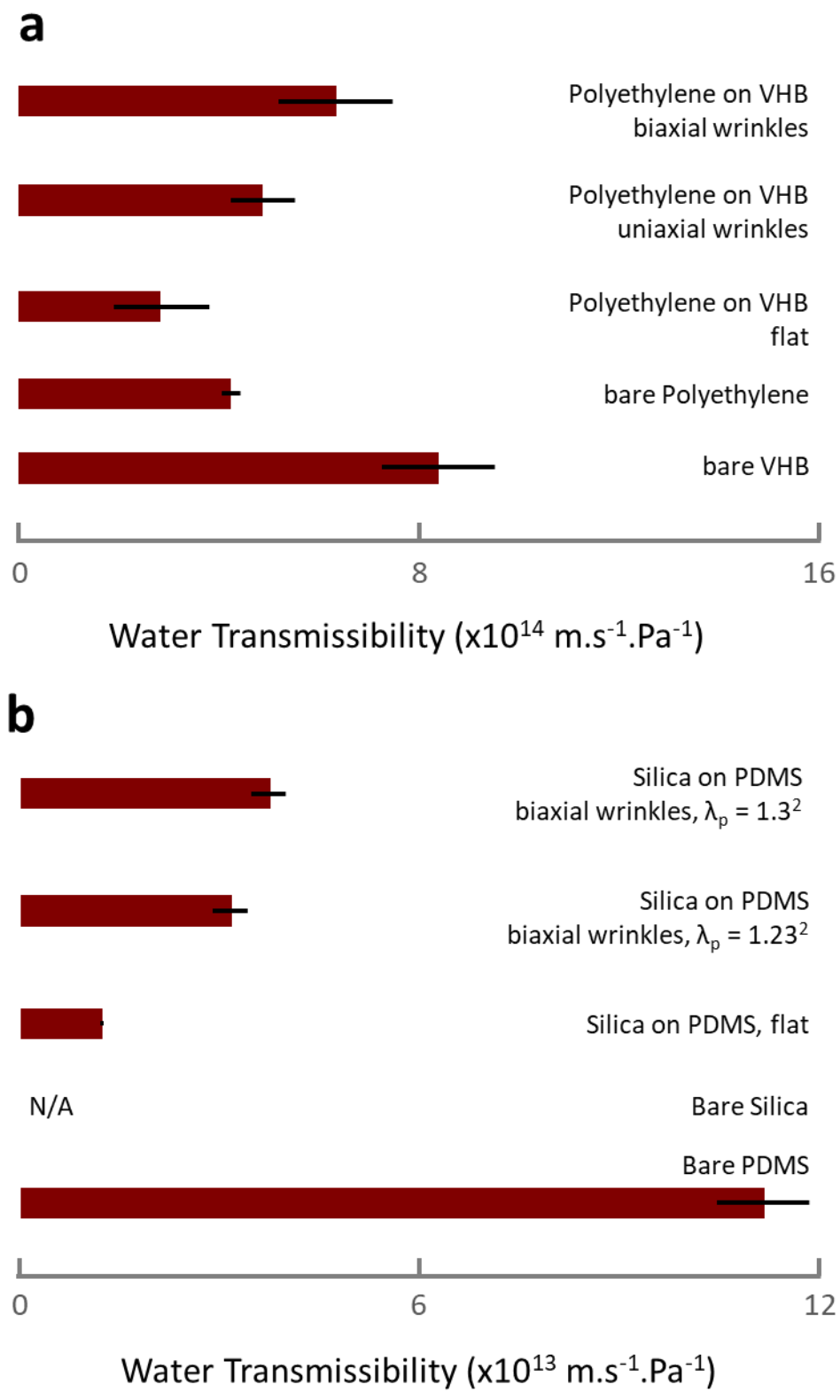

Figure 6. **The effective water transmissibility of wrinkled laminates is reduced compared to the bare substrate. a**, Polyethylene (27 μm) on VHB (500 μm). The uniaxial pre-stretch of the VHB substrate is 4, and the residual uniaxial stretch 1.75. The biaxial pre-stretch of the

VHB substrate is 3.25x3.25, and the residual biaxial stretch is 1.75x1.75. **b**, Silica (5 nm) on PDMS (200 μm). The biaxial pre-stretch of the PDMS substrate is 1.23x1.23 or 1.30x1.30. The residual biaxial stretch is negligible in this case.

Fatigue of transmissibility properties. We ascertained that the transmissibility of a wrinkled laminate remained low after cyclic loading. We prepared two uniaxially wrinkled laminates under the same experimental conditions. One laminate is a control sample, while the other is undergoing a uniaxial tension fatigue test. We repeat this procedure for two biaxially wrinkled laminates. For the polyethylene/VHB system, for the uniaxially wrinkled samples, the uniaxial pre-stretch is 4 and the residual uniaxial stretch is 1.75. For the biaxially wrinkled samples, the biaxial pre-stretch is 3.25x3.25 and the residual biaxial stretch is 1.75x1.75. We first measure the water transmissibility of all the samples simultaneously (Figure 7a, S9a). After a week of testing, we proceed to a first fatigue test (1000 cycles in uniaxial tension). We applied a uniaxial strain of 100% to uniaxially wrinkled samples, and a uniaxial strain of 50% to biaxially wrinkled samples during the fatigue test. Then we measure again the transmissibility of all the samples for another week. We next repeated this procedure for a 10000 cycles test. There is only a slight increase in the water transmissibility between the control sample and the fatigued one, even after 10000 cycles (Figure 7a, S9a). The wrinkles morphology is similar after 10000 cycles (Figure 7b, S9b).

Similarly, we studied the fatigue of transmissibility properties of silica/PDMS wrinkled laminates using the above procedure. The uniaxial strain applied are respectively 10% and 20% for biaxially wrinkled laminates with λ_p = 1.23x1.23 and λ_p = 1.30x1.30. The water transmissibility remained almost constant with the number of cycles (Figure 7c, S9d). The buckling pattern becomes anisotropic after 10000 cycles of uniaxial tension (Figure 7d): two preferred orientations are observed, short-range wrinkles parallel to the stretching direction,

and large-range creases perpendicular to the stretching direction. We hypothesize a mechanism of formation for this new microstructure: the initial wrinkled laminate is isotropic, and the wrinkles orientation continuously varies from perpendicular to parallel to the stretching direction. When a uniaxial strain is applied, wrinkles which are – to some degree – perpendicular to the stretching direction will flatten more than the ones which tend to be parallelly oriented to the stretching direction. Thus, when the laminate is fully strained in one direction, the remaining wrinkles are mostly parallel to the stretching direction. When the stretch is released, the system is already frustrated by the wrinkles parallel to the stretching direction, which prevent the immediate growth of perpendicular wrinkles. While further releasing the stretch, the laminate undergoes more violent modes of buckling such as creasing. Creases perpendicular to the stretching direction are formed and overlap on the parallel wrinkles (Figure S10). Despite this change in morphology, we do not observe the formation of cracks and additional defects compared to the pristine wrinkled sample, and we measure a steady water transmissibility with the number of cycles.

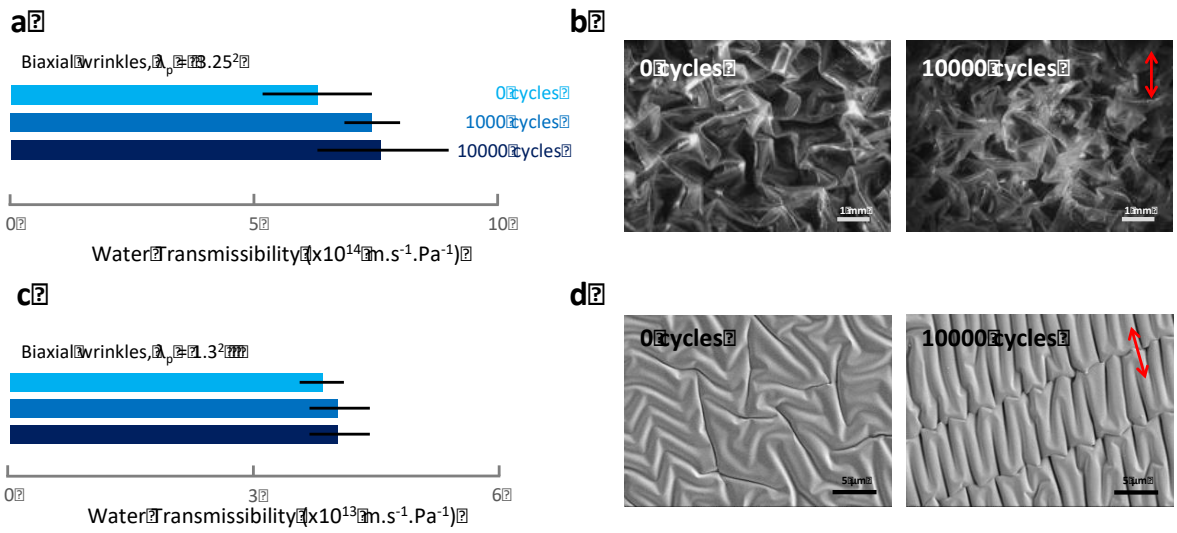

Figure 7. The transmissibility of polyethylene/VHB and silica/PDMS biaxially wrinkled laminates remains low after 10000 cycles of uniaxial tension. a, the water transmissibility

of polyethylene (27 μm)/VHB (500 μm) biaxially wrinkled laminate (λ_p = 3.25x3.25) only increases slightly with the number of cycles. The uniaxial strain applied during the fatigue test is 50%. **b,** the morphology of the plastic wrinkles is not changed after 10000 cycles. The red arrow is the direction of the strain, and the scale bars are 1 millimeter. **c,** the water transmissibility of silica (5 nm)/PDMS (200 μm) biaxially wrinkled laminate (λ_p = 1.30x1.30) only increases slightly with the number of cycles. The uniaxial strain applied during the fatigue test is 20%. **d,** biaxial silica wrinkles are anisotropic after 10000 cycles of uniaxial tension. The red arrow is the direction of the strain, and the scale bars are 5 μm.

DISCUSSIONS

If the laminate is undergoing a purely elastic deformation under cyclic stretch, the transmissibility should remain unchanged. But plastic deformations of the thin film can happen, as we observed for wrinkled aluminum. Transmissibility of wrinkled polyethylene films and wrinkled silica can sustain more than 10000 cycles of large deformation in uniaxial tension. The stress-stretch curves before and after 10000 cycles are almost identical for the uniaxially wrinkled polyethylene/VHB laminate (Figure S11a). We observed some stiffening for the biaxially wrinkled laminate (Figure S11b). We attribute this effect to the orientation of some wrinkles on the sides of the samples, parallel to the sides of the sample and the stretching direction. These wrinkles cannot be as stretchable as the ones oriented perpendicularly to the stretch direction. Thus, the plastic stiffens the composite if the stretch is too large. Again, this effect was observed principally on the sides of each sample, and may be due to edge effects during sample preparation.

In our experiment, the wrinkles morphology is not controlled, while many different patterns have been observed.[122-124] The wrinkles morphology may affect the stress concentration in the thin film, hence the damage accumulation. It is crucial to understand

stress concentration in such structures, because seals require continuous, defect-free films. Ordered wrinkles such as wrinkles with herringbone patterns lower the elastic energy, [122, 125] but it is not clear if this structure also minimize the stress concentration.

Residual stress in the stretchable seal can also have some aging effects without further stretching. Our transmissibility measurements spanned over a period of one to two months, and we did not notice any change in permeability. For practical applications, this experiment should be run over years (or under accelerated conditions, such *as* at a higher temperature). More generally speaking, the stability of biaxially wrinkled films over time should be studied in details. Mechanical stability under cyclic stretch should also be studied.

We have created wrinkles by pre-stretching the substrate, attaching a flat foil, and then releasing the substrate. In the case of polyethylene wrinkles, concomitant buckling and delamination is observed. For aluminum wrinkles on a VHB substrate and deposited silica on PDMS, delamination is almost inexistent. It is conceivable that one can create stretchable two-dimensional ordered wrinkles, such as Miura folding, by patterning the topography of the substrate or the film.[126-127] Deposition on a patterned soft substrate may enable stretchable seals without pre-stretching constraints. No matter which technique is used to prepare the wrinkles, adhesion to the substrate is of primary importance. A poor adhesion enables delamination of the foil, which can be harnessed to make large amplitude wrinkles, and reach high stretchability. A poor adhesion can, however, lower the structure resilience due to interfacial fatigue cracks.

A plurality of designs and fabrication methods can be envisioned. Some of them will be compatible with roll-to-roll, digital fabrication, and dip coating techniques. Designing stretchable seals is drawing attention towards new topics such as the fatigue of wrinkles and

the adhesion of a wrinkled film to a substrate. More generally speaking, biaxially wrinkled continuous thin films may serve new applications in stretchable electronics.

CONCLUSIONS

Long-time use of stretchable devices requires stretchable seals. At molecular level, stretchability and permeability are inextricably linked: soft and low-permeability materials do not exist. A scaling analysis shows that thin films of stiff, wrinkled, low-permeability materials can serve as stretchable seals. We have used polyethylene, aluminum and silica films as low-permeability layers, and elastomers as stretchable substrate. Wrinkled aluminum films are prone to fatigue fracture and cannot serve as stretchable seals. Wrinkled polyethylene and silica thin films demonstrate lower transmissibility than the bare elastomer and remain stretchable, and their transmissibility remains low after many cycles of stretch. We hope this work will stimulate the development of seals for stretchable devices.

MATERIALS

VHB (4905; 3M) was purchased from McMaster-Carr. Glad Press'N Seal Food Plastic Wrap was used to make polyethylene/VHB laminates. Press'N Seal is a polyethylene thin film containing no plasticizer.[128] Reynolds Wrap Heavy Duty Aluminum Foil was used to make VHB /aluminum/VHB laminates. For polydimethylsiloxane (Sylgard 184; Dow Corning), we used a 10:1 mixing ratio of precursor to curing agent. PDMS thin films were spin coated onto the backside of plastic petri dishes of various diameters. A typical recipe to make a thin film about 200 μm thick consists in spinning at 300 rpm for 80s. PDMS films were cured overnight at 65°C, and then degased for 12h in a vacuum chamber. Silica was deposited by plasma-enhanced chemical vapor deposition (PECVD), using a Cirrus 150 machine from Nexx Systems. The substrate temperature was maintained below 140°C (but is not exactly

known), by helium backcooling. Deposition pressure was maintained at 10 mTorr, with a microwave power of 300 W. Silane and dioxygen flows were respectively maintained at 50 and 20 sccm during deposition. The growth rate is about 10.5 nm/min, from previous calibrations on the same machine. The chamber can host samples as large as 5 inches in diameter. The maximum thickness of the sample inserted in the machine is about 1 cm, which allowed us to insert a homemade sample holder to apply a pre-stretch during deposition.

To measure water-transmissibility of materials, we use exactly the same dry-cup set-up fabricated for our previous work.[22] The thickness of each film (besides silica) was measured (using a vernier scale, 10 μm precision). Thin films of Press'N Seal and aluminum were folded multiple times to measure the thickness more precisely. We measured the thickness of 20 samples of each material, and values indicated the main text are "average value ± 1 standard deviation". Absolute error bars for Figures 6 and 7 represent the standard deviation of the water transmissibility measurements. The water transmissibility was determined once a day based on mass variations of the cups, for at least 7 days in a row. We study the stress-stretch behavior in uniaxial tension. A thin sheet of sample, of a long rectangular shape (usually 50 x 60 x 0.5 mm^3), was fixed to rigid grips, and mounted in a tensile tester (Instron model 5966) with a 500 N load cell. The strain rate was about 0.03 s^{-1} for the mechanical characterization in Figure 7, S5 and S6, and about 0.17 s^{-1} for the fatigue test in Figure S6.

Scanning Electron Microscopy images were taken using an Ultra55 Field Emission Scanning Electron Microscope from Zeiss. Samples were first metallized by depositing a 5 nm thick layer of Platinum / Palladium, using a HAR 050 EMS 300T D dual Head sputter coater.

ASSOCIATED CONTENT

Supporting Information

Permeability of materials, stiffness-transmissibility trade-off for laminate and brick-mortar composites, analogy with the bending of an elastica, mechanical testing of polyethylene and aluminum wrinkles, model for the transmissibility of a wrinkled laminate, fatigue of wrinkled laminates in uniaxial tension.

AUTHOR INFORMATION

Corresponding Author

suo@seas.harvard.edu

ACKNOWLEDGMENT

This work was performed in part at the Center for Nanoscale Systems (CNS), a member of the National Nanotechnology Coordinated Infrastructure (NNCI), which is supported by the National Science Foundation under NSF award no. 1541959. CNS is part of Harvard University.

Funding Sources

The work at Harvard is supported by the NSF MRSEC (DMR- 1420570). JT acknowledges the support of NSFC (No. 11702208) and the National Postdoctoral Program for Innovative Talents (No. BX201700192). J. Liu was supported by China Scholarship Council as a visiting scholar for two years at Harvard University.

REFERENCES

1. Robertson, G. L., Food Packaging: Principle and Practices Third ed.; CRC Press 2013.
2. Chung, D. D. L., Materials for Electronic Packaging Butterworth-Heinemann 1995.
3. Choi, M.-C.; Kim, Y.; Ha, C.-S., Polymers for Flexible Displays: From Material Selection to Device Applications *Progress in Polymer Science* 2008, 33 (6), 581-630.
4. Haworth, J. P.; Baldwin, F. P., Butyl Rubber Properties and Compounding *Industrial & Engineering Chemistry Research* 1942, 34 (11), 1301-1308.
5. Kim, D.-H.; Rogers, J. A., Stretchable Electronics: Materials Strategies and Devices *Advanced Materials* 2008, 20 (24), 4887-4892.
6. Rogers, J. A.; Someya, T.; Huang, Y., Materials and Mechanics for Stretchable Electronics *Science* 2010, 327.
7. Sekitani, T.; Someya, T., Stretchable, large-area Organic Electronics *Adv Mater* 2010, 22 (20), 2228-2246.

8. Hammock, M. L.; Chortos, A.; Tee, B. C.; Tok, J. B.; Bao, Z., 25th anniversary article: The Evolution of Electronic Skin (e-skin): a brief history, design considerations, and recent progress *Adv Mater* 2013, 25 (42), 5997-6038.
9. Chortos, A.; Liu, J.; Bao, Z., Pursuing Prosthetic Electronic Skin *Nat Mater* 2016, 15 (9), 937-950.
10. Sekitani, T.; Noguchi, Y.; Hata, K.; Fukushima, T.; AIda, T.; Someya, T., A Rubberlike Stretchable Active Matrix Using Elastic Conductors *Science* 2008, 321, 1468-1472.
11. Shepherd, R. F.; Ilievski, F.; Choi, W.; Morin, S. A.; Stokes, A. A.; Mazzeo, A. D.; Chen, X.; Wang, M.; Whitesides, G. M., Multigait Soft Robot *Proc Natl Acad Sci U S A* 2011, 108 (51), 20400-20403.
12. Tolley, M. T.; Shepherd, R. F.; Mosadegh, B.; Galloway, K. C.; Wehner, M.; Karpelson, M.; Wood, R. J.; Whitesides, G. M., A Resilient, Untethered Soft Robot *Soft Robotics* 2014, 1 (3), 213-223.
13. Wang, C.; Sim, K.; Chen, J.; Kim, H.; Rao, Z.; Li, Y.; Chen, W.; Song, J.; Verduzco, R.; Yu, C., Soft Ultrathin Electronics Innervated Adaptive Fully Soft Robots *Adv Mater* 2018, 30, 1706695.
14. Yang, C.; Suo, Z., Hydrogel Ionotronics *Nature Reviews Materials* 2018, 3, 125-142.
15. Kim, D. H.; Ghaffari, R.; Lu, N.; Rogers, J. A., Flexible and Stretchable Electronics for Biointegrated Devices *Annu Rev Biomed Eng* 2012, 14, 113-28.
16. Rogers, J. A.; Ghaffari, R.; Kim, D.-H., Stretchable Bioelectronics for Medical Devices and Systems Springer 2016, 1-317.
17. Han, J.; Lee, J. Y.; Lee, J.; Yeo, J. S., Highly Stretchable and Reliable, Transparent and Conductive Entangled Graphene Mesh Networks *Adv Mater* 2018, 30 (3), 1704626.
18. Dickey, M. D.; Chiechi, R. C.; Larsen, R. J.; Weiss, E. A.; Weitz, D. A.; Whitesides, G. M., Eutectic Gallium-Indium (EGaIn): A Liquid Metal Alloy for the Formation of Stable Structures in Microchannels at Room Temperature *Advanced Functional Materials* 2008, 18 (7), 1097-1104.
19. Celle, C.; Cabos, A.; Fontecave, T.; Laguitton, B.; Benayad, A.; Guettaz, L.; Pélissier, N.; Nguyen, V. H.; Bellet, D.; Muñoz-Rojas, D.; Simonato, J.-P., Oxidation of Copper Nanowire based Transparent Electrodes in ambient Conditions and their Stabilization by Encapsulation: Application to Transparent Film Heaters *Nanotechnology* 2018, 29 (8), 085701.
20. Wang, Y.; Zhu, C.; Pfattner, R.; Yan, H.; Jin, L.; Chen, S.; Molina-Lopez, F.; Lissel, F.; Liu, J.; Rabiah, N. I.; Chen, Z.; Chung, J. W.; Linder, C.; Toney, M. F.; Murmann, B.; Bao, Z., A highly Stretchable, Transparent, and Conductive Polymer *Science Advances* 2017, 3.
21. Kawano, K.; Pacios, R.; Poplavskyy, D.; Nelson, J.; Bradley, D. D. C.; Durrant, J. R., Degradation of Organic Solar Cells due to Air Exposure *Solar Energy Materials and Solar Cells* 2006, 90 (20), 3520-3530.
22. Le Floch, P.; Yao, X.; Liu, Q.; Wang, Z.; Nian, G.; Sun, Y.; Jia, L.; Suo, Z., Wearable and Washable Conductors for Active Textiles *ACS Appl Mater Interfaces* 2017, 9 (30), 25542-25552.
23. Lacour, S. P.; Jones, J.; Wagner, S.; Teng, L.; Zhigang, S., Stretchable Interconnects for Elastic Electronic Surfaces *Proceedings of the IEEE* 2005, 93 (8), 1459-1467.
24. Jones, J.; Lacour, S. P.; Wagner, S.; Suo, Z., Stretchable Wavy Metal Interconnects *J. Vac. Sci. Technol. A* 2004, 22 (4), 1723-1725.

25. Song, J.; Jiang, H.; Liu, Z. J.; Khang, D. Y.; Huang, Y.; Rogers, J. A.; Lu, C.; Koh, C. G., Buckling of a Stiff Thin film on a Compliant Substrate in Large Deformation *International Journal of Solids and Structures* 2008, 45 (10), 3107-3121.
26. Sun, Y.; Choi, W. M.; Jiang, H.; Huang, Y. Y.; Rogers, J. A., Controlled Buckling of Semiconductor Nanoribbons for Stretchable Electronics *Nat Nanotechnol* 2006, 1 (3), 201-207.
27. Li, T.; Suo, Z.; Lacour, S. P.; Wagner, S., Compliant Thin film Patterns of Stiff Materials as Platforms for Stretchable Electronics *Journal of Materials Research* 2005, 20 (12), 3274-3277.
28. Kim, D.-H.; Lu, N.; Ma, R.; Kim, Y.-S.; Kim, R.-K.; Wang, S.; Wu, J.; Won, S. M.; Tao, H.; Islam, A.; Yu, K. J.; Kim, T.-I.; Chowdhury, R.; ying, M.; Xu, Z.; Li, M.; Chung, H.-J.; Keum, H.; McCormick, M.; Liu, P.; Zhang, Y.-W.; Omenetto, F. G.; Huang, Y.; Coleman, T.; Rogers, J. A., Epidermal Electronics *Science* 2011, 333 (838-843).
29. Lipomi, D. J.; Tee, B. C.; Vosgueritchian, M.; Bao, Z., Stretchable Organic Solar Cells *Adv Mater* 2011, 23 (15), 1771-1775.
30. Lipomi, D. J.; Bao, Z., Stretchable, Elastic Materials and Devices for Solar Energy Conversion *Energy & Environmental Science* 2011, 4 (9), 3314.
31. Oh, J.-Y.; Rondeau-Gagné, S.; Chortos, A.; Lissel, F.; Wang, G.-J.; Schroeder, B. C.; Kurosawa, T.; Lopez, J.; Katsumata, T.; Xu, J.; Zhu, C.; Gu, X.; Bae, W.-G.; Kim, Y.; Jin, L.; Chung, J. W.; Tok, J. B.-H.; Bao, Z., Intrinsically Stretchable and Healable Semiconducting Polymer for Organic Transistors *Nature* 2016, 539, 411-415.
32. Hong, S.; Lee, H.; Lee, J.; Kwon, J.; Han, S.; Suh, Y. D.; Cho, H.; Shin, J.; Yeo, J.; Ko, S. H., Highly Stretchable and Transparent Metal Nanowire Heater for Wearable Electronics Applications *Adv Mater* 2015, 27 (32), 4744-4751.
33. Huang, G.-W.; Xiao, H.-M.; S-Y., F., Wearable Electronics of Silver-Nanowire/Poly(dimethylsiloxane) Nanocomposite for Smart Clothing *Scientific Reports* 2015, 5, 13971.
34. Han, S.; Hong, S.; Ham, J.; Yeo, J.; Lee, J.; Kang, B.; Lee, P.; Kwon, J.; Lee, S. S.; Yang, M. Y.; Ko, S. H., Fast Plasmonic Laser Nanowelding for a Cu-nanowire Percolation Network for Flexible Transparent Conductors and Stretchable Electronics *Adv Mater* 2014, 26 (33), 5808-5814.
35. Xu, F.; Zhu, Y., Highly Conductive and Stretchable Silver Nanowire Conductors *Adv Mater* 2012, 24 (37), 5117-5122.
36. Zang, J.; Ryu, S.; Pugno, N.; Wang, Q.; Tu, Q.; Buehler, M. J.; Zhao, X., Multifunctionality and Control of the Crumpling and Unfolding of Large-area Graphene *Nat Mater* 2013, 12 (4), 321-325.
37. Compañ, V.; Andrio, A.; López-Alemany, A.; Riande, E.; Refojo, M. F., Oxygen Permeability of Hydrogel Contact Lenses with Organosilicon Moieties *Biomaterials* 2002, (23), 2767-2772.
38. Anseth, K. S.; Bowman, C. N.; Brannon-Peppas, L., Mechanical Properties of Hydrogels and their Experimental Determination *Biomaterials* 1996, (17), 1647-1657.
39. Lin, S.; Cao, C.; Wang, Q.; Gonzalez, M.; Dolbow, J. E.; Zhao, X., Design of Stiff, Tough and Stretchy Hydrogel Composites via Nanoscale Hybrid Crosslinking and Macroscale Fiber Reinforcement *Soft Matter* 2014, 10 (38), 7519-7527.
40. Wise, D. L.; Houghton, G., The Diffusion Coefficient of ten slightly Soluble Gases in Water at 10-60°C *Chemical Engineering Science* 1966, 21, 999-1010.
41. Carpenter, J. H., New Measurement of Oxygen Solubility in Pure and Natural Water *Limnology and oceanography* 1966.

42. Tromans, D., Modeling Oxygen Solubility in Water and Electrolyte Solutions *Industrial & Engineering Chemistry Research* 2000, 39, 805-812.
43. Agache, P. G.; Monneur, C.; Leveque, J. L.; De Rigal, J., Mechanical Properties and Young's Modulus of Human Skin in Vivo *Archives of Dermatological Research* 1980, 269, 221-232.
44. Scheuplein, R. J., Handbook of Physiology, Reactions to Environmental Agents. 1977.
45. Ashby, M. F., Materials Selection in Mechanical Design fourth ed.; Elsevier 2011.
46. Department, U. o. C. E., Materials Databook 2003.
47. Helander, R. D.; Tolley, W. B. In Water Vapor Transmission Rate (WVTR) of Elastomeric Materials, Technology Vectors: 29th National SAMPE Symposium and Exhibition, MGM Grand Hotel, Reno, Nevada, April 3-5; MGM Grand Hotel, Reno, Nevada, 1984; pp 1373-1383.
48. Wolff, E. G., Introduction to the Dimensional Stability of Composite Materials 1 ed.; DEStech Publication 2004.
49. Van Amerongen, G. J., The Permeability of Different Rubbers to Gases and Its Relation to Diffusivity and Solubility *Journal of Applied Physics* 1946, 17 (11), 972-985.
50. Van Amerongen, G. J., Influence of Structure of Elastomers on Their Permeability to Gases *Journal of Polymer Science* 1949, V (3), 307-332.
51. Iyengar, Y., Relation of Water Vapor Permeability of Elastomers to Molecular Structure *Polymer Letters* 1965, 3, 663-669.
52. Robeson, L. M., Polymer Membranes for Gas Separation *Current Opinion in Solid State and Materials Science* 1999, 4, 549-552.
53. McKeen, L. W., Permeability Properties of Plastics and Elastomers Third ed.; Matthew Deans Elsevier, 2012.
54. Illinger, J. L.; Schneider, N. S.; Karasz, F. E., Water Vapor Transport in Hydrophilic Polyurethanes. In Permeability of Plastic Films
and Coatings, 1974; p 183–196.
55. 3M, VHB Tape Speciality Tapes 3M, Ed. 2014.
56. Kamal, M. R.; Jinnah, I. A.; Utracki, L. A., Permeability of Oxygen and Water Vapor Through Polyethylene/Polyamide Films *Polymer Engineering & Science* 1984, 24 (17), 1337-1347.
57. Caballero, B.; Trugo, L.; Finglas, P. M., Encyclopedia of Food Sciences and Nutrition Second ed.; Academic Press 2003.
58. Massey, L. K., Permeability Properties of Plastics and Elastomers Plastics Design Library / William Andrew Publishing 2003.
59. Lange, J.; Wyser, Y., Recent Innovations in Barrier Technologies for Plastic Packaging - a Review *Packag. Technol. Sci.* 2003, 16, 149-158.
60. Tsai, M.-H.; Tseng, I. H.; Liao, Y.-F.; Chiang, J.-C., Transparent Polyimide Nanocomposites with Improved Moisture Barrier using Graphene *Polymer International* 2013, 62 (9), 1302-1309.
61. Jung, S.-Y.; Paik, K.-W., Effects of Alignment of Graphene Flakes on Water Permeability of Graphene-epoxy Composite Film In Electronic Components & Technology Conference, IEEE 64th, IEEE: Orlando, FL, USA, 2014.
62. Huang, H.-D.; Ren, P.-G.; Chen, J.; Zhang, W.-Q.; Ji, X.; Li, Z.-M., High Barrier Graphene Oxide nanosheet/Poly(vinyl alcohol) Nanocomposite Films *Journal of Membrane Science* 2012, 409-410, 156-163.
63. Shorgen, R., Water Vapor Permeability of Biodegradable Polymers *Journal of Environmental Polymer Degradation* 1997, 5 (2), 91-95.

64. TECH, P., Parylene properties.
65. APG, Permeability of Teflon FEP Resins.
66. Schweitzer, P. A., Mechanical and Corrosion-Resistant Properties of Plastics and Elastomers Marcel Dekker 2000.
67. Matbase (online database) https://www.matbase.com/ (accessed March 17th).
68. Matweb (online database) http://www.matweb.com/index.aspx (accessed March 17th).
69. Visweswaran, B.; Mandlik, P.; Mohan, S. H.; Silvernail, J. A.; Ma, R.; Sturm, J. C.; Wagner, S., Diffusion of Water into Permeation Barrier Layers *Journal of Vacuum Science & Technology A: Vacuum, Surfaces, and Films* 2015, 33 (3), 031513.
70. Hanada, T.; Negishi, T.; Shiroishi, I.; Shiro, T., Plastic Substrate with Gas Barrier Layer and Transparent Conductive Oxide Thin Film for Flexible Displays *Thin Solid Films* 2010, 518 (11), 3089-3092.
71. Wuu, D. S.; Lo, W. C.; Chiang, C. C.; Lin, H. B.; Chang, L. S.; Horng, R. H.; Huang, C. L.; Gao, Y. J., Plasma-Deposited Silicon Oxide Barrier Films on Polyethersulfone Substrates: Temperature and Thickness Effects *Surface and Coatings Technology* 2005, 197 (2-3), 253-259.
72. Itoh, Y.; Tadashi, N., Solubility and Diffusion Coefficient of Oxygen in Silicon *Japanese Journal of Applied Physics* 1985, 24 (3), 279-284.
73. Mikkelsen, J. R., The Diffusivity and Solubility of Oxygen in SIlicon *Mat. Res. Soc. Symp. Proc.* 1985, 59, 19-30.
74. Tsai, M.-H.; Wang, H.-Y.; Lu, H.-T.; Tseng, I.-H.; Lu, H.-H.; Huang, S.-L.; Yeh, J.-M., Properties of Polyimide/Al2O3 and Si3Ni4 Deposited Thin Films *Thin Solid Films* 2011, (519), 4969-4973.
75. Andringa, A. M.; Perrotta, A.; de Peuter, K.; Knoops, H. C.; Kessels, W. M.; Creatore, M., Low-Temperature Plasma-Assisted Atomic Layer Deposition of Silicon Nitride Moisture Permeation Barrier Layers *ACS Appl Mater Interfaces* 2015, 7 (40), 22525-22532.
76. Dameron, A. A.; Davidson, D. D.; Burton, B. B.; Carcia, P. F.; McLean, R. S.; George, S. M., Gas Diffusion Barriers on Polymers Using Multilayers Fabricated by Al2O3 and Rapid SiO2 Atomic Layer Deposition *J. Phys. Chem. C* 2008, (112), 4573-4580.
77. Park, J.-S.; Chae, H.; Chung, H. K.; Lee, S. I., Thin Film Encapsulation for Flexible AM-OLED: a Review *Semiconductor Science and Technology* 2011, 26 (3), 034001.
78. Chatham, H., Oxygen Diffusion Barrier Properties of Transparent Oxide Coatings on Polymeric Substrates *Surface and Coatings Technology* 1994, (78), 1-9.
79. AZoM (online database) https://www.azom.com/ (accessed March 17th).
80. Seethamraju, S.; Kumar, S.; B, K. B.; Madras, G.; Raghavan, S.; Ramamurthy, P. C., Million-Fold Decrease in Polymer Moisture Permeability by a Graphene Monolayer *ACS Nano* 2016, 10 (7), 6501-6509.
81. Lee, C.; Wei, X.; Kysar, J. W.; Hone, J., Measurement of the Elastic Properties and Intrinsic Strength of Monolayer Graphene *Science* 2008, 321 (5887), 385-388.
82. Pierleoni, D.; Xia, Z. Y.; Christian, M.; Ligi, S.; Minelli, M.; Morandi, V.; Doghieri, F.; Palermo, V., Graphene-based Coatings on Polymer Films for Gas Barrier Applications *Carbon* 2016, 96, 503-512.
83. Chemours, Viton A-401C Fluoroelastomers 2016.
84. Peijs, T.; Van Vught, R.; Govaert, L., Mechanical Properties of Poly(vinyl Alcohol) Fibres and Composites *Composites* 1995, 26 (2), 83-90.
85. Meyer, J.; Schmidt, H.; Kowalsky, W.; Riedl, T.; Kahn, A., The Origin of Low Water Vapor Transmission Rates Through Al2O3/ZrO2 Nanolaminates Gas-diffusion

Barriers Grown by Atomic Layer Deposition *Applied Physics Letters* 2010, 96 (24), 117.
86. Dollinger, F.; Nehm, F.; Müller-Meskamp, L.; Leo, K., Laminated Aluminum Thin-Films as Low-Cost Opaque Moisture Ultra-Barriers for Flexible Organic Electronic Devices *Organic Electronics* 2017, 46, 242-246.
87. Rogers, C. E., Permeability and Chemical Resistance. In Engineering Design for Plastics, Baer, E., Ed. Van Nostrand-Reinhold: Princeton, 1964.
88. Norton, F. J., Permeation of Gaseous Oxygen through Vitreous Silica *Nature* 1961, 4789, 701.
89. Jamieson, E. H. H.; Windle, A. H., Structure and Oxygen-Barrier Properties of Metallized Polymer Film *Journal of Materials Science* 1983, 18, 64 - 80.
90. Leterrier, Y., Durability of Nanosized Oxygen-Barrier Coatings on Polymers *Progress in Materials Sciences* 2003, 48, 1-55.
91. Miller, K. S.; Krochta, J. M., Oxygen and Aroma Barrier Properties of Edible Films: A Review *Trends in Food Science & Technology* 1997, 8 (7), 228-237.
92. Ryder, L., OXYGEN-BARRIER CONTAINERS-THEIR DESIGN AND COST *PLASTICS ENGINEERING* 1984, 40 (5), 41-48.
93. Brandrup, J.; Immergut, E. H.; Grulke, E. A.; Abe, A.; Bloch, D. R., Polymer Handbook Wiley New York etc 1989; Vol. 7.
94. Tropsha, Y. G. H., N. G., Activated Rate Theory Treatment of Oxygen and Water Transport through Silicon Oxide/ Poly(ethylene terephthalate) Composite Barrier Structures *J. Phys. Chem. B* 1997, 101, 2259-2266.
95. Czeremuszkin, G. K.-S., J.E.
Wertheimer, M. R., Transparent Barrier Coatings on Polyethylene Terephthalate by Single- and Dual-Frequency Plasma-Enhanced Chemical Vapor Deposition *J. Vac. Sci. Technol. A* 1998, 16 (6), 3190-3198.
96. Slee, J. A.; Orchard, G. A. J.; Bower, D. I.; Ward, I. M., The Transport of Oxygen Through Oriented Poly(ethylene terephthalate) *Journal of Polymer Science Part B: Polymer Physics* 1989, 27 (1), 71-83.
97. Hernandez, R. J., Effect of Water Vapor on the Transport Properties of Oxygen through Polyamide Packaging Materials. In Water in Foods, Pergamon: Amsterdam, 1994; pp 495-507.
98. Mandlik, P., A Novel Hybrid Inorganic-Organic Single Layer Barrier for Organic Light-Emitting Diodes Princeton University 2009.
99. Roberts, A. P.; Henry, B. M.; Sutton, A. P.; Grovenor, C. R. M.; Briggs, G. A. D.; Miyamoto, T.; Kano, M.; Tsukahara, Y.; Yanaka, M., Gas Permeation in Silicon-Oxide/Polymer (SiOx/PET) Barrier Films: Role of the Oxide Lattice, Nano-Defects and Macro-Defects *Journal of Membrane Science* 2002, 208, 75-88.
100. Yanaka, M.; Henry, B. M.; Roberts, A. P.; Grovenor, C. R. M.; Briggs, G. A. D.; Sutton, A. P.; Miyamoto, T.; Tsukahara, Y.; Takeda, N.; Chater, R. J., How Cracks in SiOx-Coated Polyester Films affect Gas Permeation *Thin Solid Films* 2001, 397, 176-185.
101. Tropsha, Y. G.; Harvey, N. G., Activated Rate Theory Treatment of Oxygen and Water Transport through Silicon Oxide/ Poly(ethylene terephthalate) Composite Barrier Structures *J. Phys. Chem. B* 1997, 101, 2259-2266.
102. Vohra, A.; Filiatrault, H. L.; Amyotte, S. D.; Carmichael, R. S.; Suhan, N. D.; Siegers, C.; Ferrari, L.; Davidson, G. J. E.; Carmichael, T. B., Reinventing Butyl Rubber for Stretchable Electronics *Advanced Functional Materials* 2016, (26), 5222-5229.

103. Vohra, A.; Carmichael, R. S.; Carmichael, T. B., Developing the Surface Chemistry of Transparent Butyl Rubber for Impermeable Stretchable Electronics *Langmuir* 2016, 32 (40), 10206-10212.
104. Hauch, J. A.; Schilinsky, P.; Choulis, S. A.; Rajoelson, S.; Brabec, C. J., The Impact of Water Vapor Transmission Rate on the Lifetime of Flexible Polymer Solar Cells *Applied Physics Letters* 2008, (93), 103306.
105. Garner, S.; Glaesemann, S.; Li, X., Ultra-slim Flexible Glass for Roll-to-Roll Electronic Device Fabrication *Applied Physics A* 2014, 116 (2), 403-407.
106. Nielsen, L. E., Models for the Permeability of Filled Polymer Systems *Journal of Macromolecular Science: Part A - Chemistry* 1967, 1 (5), 929-942.
107. Bharadwaj, R. K., Modeling the Barrier Properties of Polymer-Layered Silicate Nanocomposites *Macromolecules* 2001, 34, 9189-9192.
108. Cui, Y.; Kundalwal, S. I.; Kumar, S., Gas Barrier Performance of Graphene/Polymer Nanocomposites *Carbon* 2016, 98, 313-333.
109. Suo, Z.; Ma, E. Y.; Gleskova, H.; Wagner, S., Mechanics of Rollable and Foldable Film-on-Foil Electronics *Applied Physics Letters* 1999, 74 (1177-1179).
110. Sharpe, W. N.; Pulskamp, J.; Gianola, D. S.; Eberl, C.; Polcawich, R. G.; Thompson, R. J., Strain Measurements of Silicon Dioxide Microspecimens by Digital Imaging Processing *Experimental Mechanics* 2007, 47 (5), 649-658.
111. Wiederhorn, S. M.; Fields, B. A.; Hockey, B. J., Fracture of Silicon Nitride and Silicon Carbide at Elevated Temperatures *Materials Science and Engineering: A* 1994, 176 (1-2), 51-60.
112. Euler, L., Methodus Inveniendi Lineas Curvas Maximi Minimive Proprietate Gaudentes Sive Solutio Problematis Isoperimetrici Latissimo Sensu Accepti 1744.
113. Love, A. E. H., A Treatise on The Mathematical Theory of Elastivity Cambridge University Press 1892.
114. Antman, S. S., Nonlinear Problems of Elasticity Second ed.; Springer 2005; Vol. 107.
115. Pacheco, M. E.; Piña, E., The Elastic Rod *Revista mexicana de física E* 2007, 53 (2), 186-190.
116. Audoly, B.; Pomeau, Y., Elasticity and Geometry Oxford University Press 2010.
117. Moon, M. W.; Lee, K. R.; Oh, K. H.; Hutchinson, J. W., Buckle Delamination on Patterned Substrates *Acta Materialia* 2004, 52 (10), 3151-3159.
118. Mei, H.; Landis, C. M.; Huang, R., Concomitant Wrinkling and Buckle-Delamination of Elastic Thin Films on Compliant Substrates *Mechanics of Materials* 2011, 43 (11), 627-642.
119. Bowden, N.; Brittain, S.; Evans, A. G.; Hutchinson, J. W.; Whitesides, G. M., Spontaneous Formation of Ordered Structures in Thin Films of Metals Supported on an Elastomeric Polymer *Nature* 1998, 393, 146-149.
120. Chen, X.; Hutchinson, J. W., Herringbone Buckling Patterns of Compressed Thin Films on Compliant Substrates *Journal of Applied Mechanics* 2004, 71 (5), 597.
121. JCGM, Evaluation of Measurement Data — Guide to the Expression of Uncertainty in Measurement 2008.
122. Huang, Z.; Hong, W.; Suo, Z., Evolution of Wrinkles in Hard Films on Soft Substrates *Phys Rev E Stat Nonlin Soft Matter Phys* 2004, 70 (3 Pt 1), 030601.
123. Breid, D.; Crosby, A. J., Effect of Stress State on Wrinkle Morphology *Soft Matter* 2011, 7 (9), 4490.
124. Li, B.; Cao, Y.-P.; Feng, X.-Q.; Gao, H., Mechanics of Morphological Instabilities and Surface Wrinkling in Soft Materials: a Review *Soft Matter* 2012, 8 (21), 5728.

125. Cai, S.; Breid, D.; Crosby, A. J.; Suo, Z.; Hutchinson, J. W., Periodic Patterns and Energy States of Buckled Films on Compliant Substrates *Journal of the Mechanics and Physics of Solids* 2011, 59 (5), 1094-1114.
126. Song, Z.; Ma, T.; Tang, R.; Cheng, Q.; Wang, X.; Krishnaraju, D.; Panat, R.; Chan, C. K.; Yu, H.; Jiang, H., Origami Lithium-Ion Batteries *Nat Commun* 2014, 5, 3140.
127. Miura, K. Method of Packaging and Deployment of Large Membranes in Space; 1985.
128. Glad Products FAQs https://www.glad.com/faq/ (accessed March 17th).

Table of Contents Only

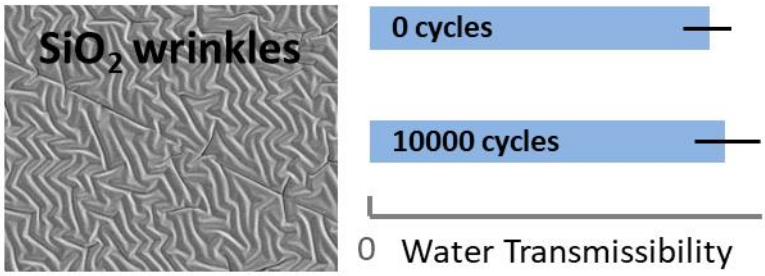

Supporting information
Stretchable Seal

Paul Le Floch[1#], Shi Meixuanzi[2#], Jingda Tang[2], Junjie Liu[1, 3], Zhigang Suo[1*]

[1]School of Engineering and Applied Sciences, Kavli Institute for Bionano Science and Technology, Harvard University, MA 02138

[2]State Key Lab for Strength and Vibration of Mechanical Structures, Department of Engineering Mechanics, Xi'an Jiaotong University, Xi'an 710049, China

[3]State Key Laboratory of Fluid Power & Mechatronic System, Key Laboratory of Soft Machines and Smart Devices of Zhejiang Province, and Department of Engineering Mechanics, Zhejiang University, Hangzhou 310027, China

[#]Those authors contributed equally to this work.

*Corresponding author: suo@seas.harvard.edu

Permeability of materials

The permeability of a film is defined with equation (1). The flux J is a number of molecules per unit area and per unit time. $\Delta\prod$ is the difference of pressure between both sides of a film of material, which has a thickness h. Thus, the permeability P has the following dimension:

$$P = J\frac{h}{\Delta P} = \frac{(number)}{(area)*(time)}\frac{(length)}{(pressure)} \qquad (1)$$

If the number of molecules is expressed as a volume in a standard state (for instance, ambient temperature at one atmosphere pressure), the S.I. unit of permeability is "$m^2.s^{-1}.Pa^{-1}$". In the literature, the oxygen permeability is very often expressed using this system of units. In case of water vapor, the number of molecules is more likely to be expressed as a mass rather than a volume. To convert a water flux or a transmission rate to a permeability with the unit "$m^2.s^{-1}.Pa^{-1}$", we simply use the fact that the density of water is 10^3 $kg.m^{-3}$ in the standard state.

When the literature only provides the flux – also called Water Vapor Transmission Rate (WVTR), or Oxygen Transmission Rate (OTR) – it is needed to know both h and $\Delta\prod$ to calculate P. $\Delta\prod$ depends on the measurement method. In most cases, one side of the film the ambient atmosphere, while the other side is a closed chamber where humidity or oxygen concentration are maintained to some much lower levels. For instance, $\prod$ = 3.2 kPa for water vapor, and 21 kPa for oxygen in the atmosphere, in standard conditions of pressure and temperature. WVTR measurements can be done at various temperatures, and at various values of relative humidity (Table S1). We take into account that partial pressures vary with temperature to build Table S1 and Figure 1. In the literature, the oxygen permeability (or transmissibility) can also be

expressed “per atmosphere of air”. In Table S1, we always give oxygen permeability values in standard units (“$m^2.s^{-1}.Pa^{-1}$”).

Different standard conditions can be used to measure WVTR and OTR of materials. The temperature of measurement can notably vary between 23 and 40°C. It has been shown that permeation is a thermally activated process,[1] and that

$$P = P_0 e^{-\frac{Q}{RT}} \qquad (2)$$

Where Q is activation energy of permeation (usually expressed in kJ/mol), and P_0 is a constant. By choosing a very low value for the activation energy, we can estimate an upper bound for the relative change in permeability due to temperature. We choose Q = 21 kJ/mol (≈ 5 kcal/mol), which is a very low value for oxygen permeation in an elastomer.[1] For T_1 = 23°C and T_2 = 40°C, $e^{-\frac{Q}{R}\left(\frac{1}{T_2}-\frac{1}{T_1}\right)} \cong 1.6$. The relative change in permeability in this range of temperature is small compared to the scattering between data from various literature sources. Thus, we decided to plot all data points corresponding to this range of temperature in single charts (Figure 1, 2 and 3).

Table S1. Elastic modulus and permeability of materials.

Material	**Elastic Modulus (Pa)**	**Water Permeability (m^2/Pa/s)**	**Remarks on Water Permeability**	**Oxygen Permeability (m^2/Pa/s)**	**Remarks on Oxygen Permeability**
Hydrogels	10^3-10^7 [2-3]	$7.26*10^{-13}$	We take the water-diffusivity of the hydrogel equal to the self-diffusion coefficient of pure water with a standard value of $2.3*10^{-9}$ m^2/s at 25°C. We take the water-solubility equal to 1/3169	$6.99*10^{-16}$ [4-5]	Partial pressure of oxygen is about 21 kPa and the liquid water is in equilibrium with the saturated vapor (R.H. = 100%). We interpolate Wise's table to get the diffusion coefficient of oxygen at 25°C, equal to $2.55*10^{-9}$$m^2$/s

			m3/m3/Pa at 25°C.	$7.43*10^{-16}$ [4, 6]	Use of Tromans[6] data: Figure 10 gives us the solubility of oxygen in pure water at 25°C. To convert the solubility from mol(O_2)/kg(H_2O)/atm to standard units of solubility ($m^3/m^3/Pa$), we use 1 atm = 10^5Pa and a molar volume of oxygen equal to 22.4 L/mol
Skin	$4.2*10^5$ [7]	$1.58*10^{-13}$ [8]	The reference provides both solubility and permeability values at 25°C		
Elastomers	10^5 - 10^8 [9]				
Butyl Rubber (Poly(isobutene-isoprene))	10^6 - $2*10^6$ [9-10]	$4.79*10^{-19}$ [11]	24°C, 80% R.H. (ASTM E96-66)	$4.29*10^{-17}$ [1]	The commerical rubber used here is Oppanol B. At 25°C, for an air pressure of 1 atmosphere, the partial pressure of oxygen is about 21 kPa
		$1.16*10^{-18}$ [12]	ASTM E96-80	$4.71*10^{-17}$ [13]	
		$2.56*10^{-18}$ [14]	23°C, 100% R.H.		
		$3.34*10^{-18}$ [14]	23°C, 100% R.H.		
		$1.89*10^{-18}$ [15]	We suppose that the vapor pressure is 3169 Pa		
		$1.13*10^{-18}$ [16]	p684, Table A-IV. 39°C, 90% R.H.		
Silicone Rubber	$5*10^6$ - $2*10^7$ [9]	$1.62*10^{-16}$ [11]	24°C, 80% R.H. (ASTM E96-66)	$5.86*10^{-15}$ [17]	
		$3.10*10^{-16}$ [12]	ASTM E96-80	$4.65*10^{-16}$ [18]	
		$2.67*10^{-16}$ [14]	23°C, 100% R.H.		
Fluorosilicone Rubber		$1.10*10^{-16}$ [11]	24°C, 80% R.H. (ASTM E96-66)		

Polyurethane	$2^{*}\ 10^{6}$ - $4^{*}\ 10^{7}$ [8,9][9-10]	$2.37^{*}10^{-16}$ [12]	ASTM E96-80. Sample "Polyester urethene"	$8.93^{*}10^{-15}$ [18]	Hypothesis: the data have a pressure unit of atm^{-1}. We suppose that the corresponding partial pressure of oxygen is 21000 Pa. Material: Lubrizol Estane (Thermoplastic Urethane)
		$1.59^{*}10^{-16}$ [12]	ASTM E96-80. Sample "ADIPRENE"		
		$4.07^{*}10^{-15}$ [19]	30°C, 50% R.H. Sample "10PE33", by multiplying diffusivity and solubility, and dividing by the pressure difference		
		$4.66^{*}10^{-16}$ [19]	30°C, 50% R.H. Sample "5PE40"		
		$2.27^{*}10^{-16}$ [19]	30°C, 50% R.H. Sample "0PE33"		
VHB 4905	$1.8^{*}10^{6}$ [20]	$4.00^{*}10^{-17}$ [14]	23°C, 100% R.H.		
VHB4950		$1.16^{*}10^{-18}$ [20]	ASTM F1249 at 38°C/100% RH		
Nitrile Rubber	$2^{*}\ 10^{6}$ - $5^{*}10^{6}$ [21]	$4.63^{*}10^{-17}$ [11]	24°C, 80% R.H. (ASTM E96-66)	$2.97^{*}10^{-16}$ [13]	Perbunan 18. We suppose that one atmosphere corresponds to an oxygen partial pressure of 21000 Pa
		$6.67^{*}10^{-17}$ [12]	ASTM E96-80. Sample "NBR"	$1.4^{*}10^{-16}$ [13]	Perbunan (German). We suppose that one atmosphere corresponds to an oxygen partial pressure of 21000 Pa
		$4.5^{*}10^{-17}$ [14]	23°C, 100% R.H.	$7.99^{*}10^{-17}$ [18]	High Nitrile-content NBR. Measurement at 23°C
		$1.50^{*}10^{-17}$ [18]	High Nitrile-content NBR. Measurement at 23°C		

Natural Rubber	$1.5^{*}\ 10^{6}$ - $4^{*}10^{7}$ [9-10]	$2.50^{*}10^{-17}$ [12]	ASTM E96-80	$8.43^{*}10^{-16}$ [13]	We suppose that one atmosphere corresponds to an oxygen partial pressure of 21000 Pa
		$1.70^{*}10^{-17}$ [16]	p684, Table A-IV. 39°C, 90% R.H.		
Fluoroelastomer	$4.0^{*}10^{6}$ - $5.2^{*}10^{6}$ [22]	$4.63^{*}10^{-18}$ [11]	24°C, 80% R.H. (ASTM E96-66). Sample "VITON"		
		$1.01^{*}10^{-17}$ [12]	ASTM E96-80. Sample "VITON"		
EPDM (Ethylene Propylene Diene Monomer)	$2^{*}\ 10^{6}$ - $1^{*}10^{7}$ [21]	$3.83^{*}10^{-18}$ [11]	24°C, 80% R.H. (ASTM E96-66)		
		$6.89^{*}10^{-18}$ [12]	ASTM E96-80		
		$8.85^{*}10^{-18}$ [15]			
Polychlorobutadiene (Neoprene)	$7^{*}\ 10^{5}$ - $2^{*}10^{6}$ [10]	$7.07^{*}10^{-18}$ [11]	24°C, 80% R.H. (ASTM E96-66)		
		$2.45^{*}10^{-18}$ [12]	ASTM E96-80		
		$1.04^{*}10^{-17}$ [16]	p684, Table A-IV. 39°C, 90% R.H.		
HYPALON (chlorosulfonated polyethylene, CSPE)	$2^{*}\ 10^{6}$ - $1.5^{*}10^{7}$ [21]	$8.23^{*}10^{-18}$ [11]	24°C, 80% R.H. (ASTM E96-66)		
		$7.01^{*}10^{-18}$ [16]	p684, Table A-IV. 39°C, 90% R.H.		
		$7.66^{*}10^{-18}$ [12]	ASTM E96-80		
Chlorobutyl	$9.7^{*}10^{6}$ [23]	$1.33^{*}10^{-18}$ [12]			
Polybutadiene Rubber	$1^{*}\ 10^{6}$ - $2.2^{*}10^{6}$ [24]	$2.96^{*}10^{-17}$ [16]	p684, Table A-IV. 40°C, 90% R.H.		
Plastics					
Amorphous Polyamide	$2.62^{*}\ 10^{9}$ - $3.2^{*}10^{9}$ [10]	$1.83^{*}10^{-20}$ [18]	Water Vapor Permeation at 23 °C through EMS Chemie Grivory G16, ASTM D3985. Hypothesis: R.H.	$8.49^{*}10^{-19}$ [18]	Permeation of Oxygen at 23°C through EMS Chemie Grivory G16, ASTM D3985, at 0% R.H.

			= 100%		
		$9.65*10^{-19}$ [18]	Water Vapor at 90% RH through DuPont Selar, PA Amorphous Nylon, at 37,8°C	$1.63*10^{-18}$ [18]	Oxygen Permeation of DuPont Selar, Table 8.7, p124. T = 30°C, R.H. > 95%
Polyamide		$2.15*10^{-18}$ - $4.30*10^{-17}$ [25]	Table 1. 23°C, 85% R.H.	$5.51*10^{-20}$ - $5.51*10^{-19}$ [25]	Table 1. 23°C, 50% or 0% R.H.
Polyamide 6 (Nylon 6)	$2.3*10^{9}$ - $2.5*10^{9}$ [21]	$1.75*10^{-18}$ [18]	Water Vapor through Honeywell Plastics Capron! Nylon 6 Films. Film thickness: 0.019 mm; RH: 50%. 23°C. Table 8.9	$5.62*10^{-19}$ [18]	Permeation of Gases at Various Temperatures through Honeywell Plastics Capron Nylon 6 Films. Film thickness: 0.0254 mm; RH: 0%. 23°C. Table 8.8
		$1.55*10^{-17}$ [26]	37.8°C, 90% R.H.	$1.17*10^{-20}$ [26]	25°C, 0% R.H.
		$1.16*10^{-17}$ [27]	25°C, 75% R.H. page 4314	$5.51*10^{-19}$ [27]	23°C, dry gas. We suppose that the test is run at a pressure of 1 atmosphere
		$5.48*10^{-18}$ [16]	p684, Table A-IV. 38°C, 90% R.H.	$5.00*10^{-20}$ - $2.50*10^{-19}$ [28-31]	Standard Temperature and Pressure Conditions
Polyamide 66 (Nylon 66)	$1.7*10^{9}$ - $5.52*10^{9}$ [21, 23]	$4.30*10^{-18}$ [18]	Table 8.23 Permeation of Oxygen, Carbon Dioxide, Nitrogen, and Water Vapor at 23 C through EMS-Grivory Grilon BM 20 SBG Test Method: ISO 15105-1. 85% R.H.	$7.16*10^{-19}$ [18]	Table 8.23 Permeation of Oxygen, Carbon Dioxide, Nitrogen, and Water Vapor at 23 C through EMS-Grivory Grilon BM 20 SBG. Test Method: ISO 15105-1. 0% R.H.
				$1.92*10^{-18}$ [18]	Table 8.23 Permeation of Oxygen, Carbon Dioxide, Nitrogen, and Water Vapor at 23 C through EMS-Grivory Grilon BM 20 SBG. Test Method: ISO 15105-1. 85% R.H.
		$1.62*10^{-17}$ [26]	37.8°C, 90% R.H.	$9.08*10^{-20}$ [26]	25°C, 0% R.H.

		$2.74*10^{-18}$ [27]	25°C, 75% R.H. page 4314	$4.82*10^{-19}$ [27]	23°C, dry gas. We suppose that the test is run at a pressure of 1 atmosphere
		$9.8*10^{-18}$ [16]	p684, Table A-IV. 39°C, 90% R.H.		
Ultra low-density Polyethylene (ULDPE)		$3.42*10^{-19}$ [18]	Permeation of Water Vapor at 23 C and 50% Relative Humidity through Dow Chemical Attane Blown Film (Grade 4201). ASTM F1249. Table 9.3	$1.55*10^{-16}$ [18]	Permeation of Oxygen at 23 C and 50% Relative Humidity through Dow Chemical Attane Blown Film (Grade 4201). ASTM F1249. Table 9.1
Linear low-density Polyethylene (LLDPE)	$1.4*10^{8}$ - $1.57*10^{9}$ [21, 23]	$1.31*10^{-18}$ [18]	Permeation of Water and Oxygen through Exopack Sclairfilm LX-1 (LLDPE) Film. Table 9.4. Film Thickness, 0.0762. ASTM D3985. Hypothesis: R.H. = 100%	$1.3*10^{-16}$ [18]	Permeation of Water and Oxygen through Exopack Sclairfilm LX-1 (LLDPE) Film. Table 9.4. Film Thickness, 0.0762. ASTM D3985.
		$7.21*10^{-19}$ [26]	37.8°C, 90% R.H.	$1.92*10^{-17}$ [26]	25°C, 0% R.H.
Low-density Polyethylene (LDPE)	$1.1*10^{8}$ - $4.49*10^{8}$ [21, 23]	$1.79*10^{-16}$ [18]	Permeation of Gases at 24 C through Dow Chemical Low-Density Polyethylene. Table 9.7 (mean value). Hypothesis: R.H. = 100%	$6.50*10^{-17}$ [18]	Permeation of Gases at 24 C through Dow Chemical Low-Density Polyethylene. Table 9.6 (mean value)
		$7.75*10^{-19}$ [26]	37.8°C, 90% R.H.	$2.08*10^{-17}$ [26]	25°C, 0% R.H.
		$4.87*10^{-19}$ [27]	25°C, 75% R.H. page 4314	$1.02*10^{-16}$ [27]	23°C, dry gas. We suppose that the test is run at a pressure of 1 atmosphere
				$2.5*10^{-17}$ [28-30, 32]	Standard Temperature and Pressure Conditions

High-density Polyethylene (HDPE)	$4.5*10^{8}$ - $1.5*10^{9}$ [21, 23]	$7.67*10^{-19}$ [18]	Permeation of Oxygen and Water through NOVA Chemicals Sclair 15A HDPE Films. Test methods: ASTM E96 and ASTM D3985. Table 9.11. Hypothesis: R.H. = 100%	$5.02*10^{-17}$ [18]	Permeation of Oxygen and Water through NOVA Chemicals Sclair 15A HDPE Films. Test methods: ASTM E96 and ASTM D3985. Table 9.11
		$2.43*10^{-19}$ [26]	37.8°C, 90% R.H.	$6.25*10^{-18}$ [26]	25°C, 0% R.H.
		$1.76*10^{-19}$ [27]	25°C, 75% R.H. page 4314	$2.20*10^{-17}$ [27]	23°C, dry gas. We suppose that the test is run at a pressure of 1 atmosphere
				$5*10^{-18}$ [32]	Standard Temperature and Pressure Conditions
Polyethylene (PE)	$6.21*10^{8}$ - $8.96*10^{8}$ [10]	$2.15*10^{-18}$ - $8.59*10^{-18}$ [25]	Table 1. 23°C, 85% R.H.	$2.76*10^{-17}$ - $1.10*10^{-16}$ [25]	Table 1. 23°C, 50% or 0% R.H.
		$1.74*10^{-19}$ - $1.22*10^{-18}$ [16]	p684, Table A-IV. 37-39°C, 90% R.H., density varying from 0.92 to 0.96 g/mL		
Polypropylene	$8*10^{8}$ - $8.25*10^{9}$ [21, 23]	$4.02*10^{-19}$ [27]	PP-cast. 25°C, 75% R.H. page 4314	$4.19*10^{-17}$ [27]	PP-cast. 23°C, dry gas. We suppose that the test is run at a pressure of 1 atmosphere
		$1.64*10^{-19}$ [27]	OPP-coextruded. 25°C, 75% R.H. page 4315	$2.14*10^{-17}$ [27]	OPP-coextrude. 23°C, dry gas. We suppose that the test is run at a pressure of 1 atmosphere
		$3.79*10^{-19}$ [16]	p684, Table A-IV. 38°C, 90% R.H.	$8.32*10^{-17}$ [18]	Ineos Polypropylene. Table 9.16, p157. 30°C
				$3.25*10^{-17}$ - $5.62*10^{-17}$ [33]	Table 45-01, p284
		$8.59*10^{-19}$ - $1.72*10^{-18}$ [25]	Table 1. 23°C, 85% R.H.	$2.76*10^{-17}$ - $5.51*10^{-17}$ [25]	Table 1. 23°C, 50% or 0% R.H.
				$5.3*10^{-18}$ – $1.7*10^{-17}$ [28-30]	Standard Temperature and Pressure conditions

Polyvinylchloride (PVC)	$1.63*10^{6}$ - $3.24*10^{9}$ [23]	$1.46*10^{-18}$ [27]	PVC-rigid.25°C, 75% R.H. page 4316	$1.65*10^{-18}$ [27]	PVC-rigid. 23°C, dry gas. We suppose that the test is run at a pressure of 1 atmosphere
		$8.52*10^{-19}$ [27]	PVC-oriented. 25°C, 75% R.H. page 4317	$3.72*10^{-19}$ [27]	PVC-oriented. 23°C, dry gas. We suppose that the test is run at a pressure of 1 atmosphere
		$2.03*10^{-18}$ [18]	VPI Mirrex ® 1025 PVC. Table 9.59, p180. Test method: ASTM F372.	$2.59*10^{-18}$ [18]	VPI Mirrex ® 1025 PVC. Table 9.60, p180. Test method: Mocon Oxtran.
		$4.30*10^{-18}$ - $8.59*10^{-18}$ [25]	Table 1. 23°C, 85% R.H.	$1.10*10^{-18}$ - $4.41*10^{-18}$ [25]	Table 1. 23°C, 50% or 0% R.H.
		$1.39*10^{-18}$ - $8.71*10^{-18}$ [16]	p684, Table A-IV. 38-40°C, 90% R.H., 3 values	$5.9*10^{-20}$ [29]	Standard Temperature and Pressure conditions
Polyvinylidene chloride (PVdC)	$1.03*10^{9}$ [23]	$3.04*10^{-20}$ [27]	25°C, 75% R.H. page 4318	$1.72*10^{-20}$ - $2.00*10^{-19}$ [27]	23°C, dry gas. We suppose that the test is run at a pressure of 1 atmosphere
		$4.30*10^{-19}$ [25]	Table 1. 23°C, 85% R.H.	$5.51*10^{-21}$ - $1.65*10^{-19}$ [25]	Table 1. 23°C, 50% or 0% R.H.
		$2.81*10^{-19}$ [23]	Dow Saran® 18L Clear Plastic Barrier Film	$2.60*10^{-19}$ [23]	Dow Saran® 18L Clear Plastic Barrier Film
		$6.53*10^{-20}$ - $3.05*10^{-19}$ [16]	p684, Table A-IV. 39°C, 90% R.H.	$3.8*10^{-21}$ - $4*10^{-20}$ [29-30]	Standard Temperature and Pressure conditions
Polystyrene	$3.03*10^{9}$ - $3.35*10^{9}$ [23]	$8.52*10^{-18}$ [27]	PS-cast. 25°C, 75% R.H. page 4319	$6.20*10^{-17}$ [27]	PS-cast. 23°C, dry gas. We suppose that the test is run at a pressure of 1 atmosphere
		$2.92*10^{-18}$ - $1.42*10^{-17}$ [18]	Styron © PS. 24°C, table 5.12 page 83	$6.50*10^{-17}$ - $8.65*10^{-17}$ [18]	Styron © PS. 24°C, table 5.12 page 83
		$4.30*10^{-18}$ - $1.72*10^{-17}$ [25]	Table 1. 23°C, 85% R.H.	$5.51*10^{-17}$ - $8.27*10^{-17}$ [25]	Table 1. 23°C, 50% or 0% R.H.
		$5.79*10^{-18}$ [16]	p684, Table A-IV. 39°C, 90% R.H.	$2*10^{-17}$ [28]	Standard Temperature and Pressure conditions
Polycarbonate	$1.6*10^{9}$ - $6.00*10^{9}$ [21, 23]	$8.83*10^{-18}$ [27]	25°C, 75% R.H. page 4320	$4.41*10^{-17}$ [27]	23°C, dry gas. We suppose that the test is run at a pressure of 1 atmosphere

		$4.26*10^{-18}$ [16]	p684, Table A-IV. 20°C, 90% R.H.	$3.58*10^{-17}$ [23]	Overview of materials for Polycarbonate, Molded
				$1.05*10^{-17}$ [28]	Standard Temperature and Pressure conditions
Polyethylene Terephthalate (PET)	$1.07*10^{8}$ - $5.20*10^{9}$ [32,33]	$8.52*10^{-19}$ [27]	25°C, 75% R.H. page 4321	$7.58*10^{-19}$ [27]	23°C, dry gas. We suppose that the test is run at a pressure of 1 atmosphere
		$1.09*10^{-18}$ [18]	DuPont, Teijin Films, Mylar 800 PET Films (p102, table 6.20). 38°C, 90 % R.H.	$6.23*10^{-19}$ [18]	DuPont, Teijin Films, Mylar 800 PET Films (p102, table 6.20). 23°C, 75 % R.H.
		$2.15*10^{-18}$ - $8.59*10^{-18}$ [25]	Table 1. 23°C, 85% R.H.	$5.51*10^{-19}$ - $2.76*10^{-18}$ [25]	Table 1. 23°C, 50% or 0% R.H.
		$1.31*10^{-18}$ [16]	p684, Table A-IV. 39°C, 90% R.H.	$1*10^{-19}$ - $3*10^{-19}$ [28-30, 34-35]	Standard Temperature and Pressure conditions
		$3.11*10^{-18}$ [36]	Table 2, 30°C. We use a molar volume of 24.5 mol/L for water vapor. 100% R.H. difference. Set-up: Permatran W600 from Modern Controls.	$5.91*10^{-18}$ [36]	Permeance measurements for oxygen were obtained using a temperature-controlled OxTran 2/20 from Modern Controls, Inc. Oxygen gradient across the film system was kept at a constant 1 atm, 100% oxygen concentration on the upstream side of the film vs 1 atm, 98% nitrogen/2% hydrogen carrier gas on the downstream side. Water vapor content on both sides of the test film was kept at 0% relative humidity. Data shown here are for 30°C.
Cellulose acetate	$1.60*10^{9}$ - $2.46*10^{9}$ [23]	$4.14*10^{-19}$ [27]	Cellulosic film 445MXXT A. 25°C, 75% R.H. page 4314	$1.21*10^{-19}$ [27]	Cellulosic film 445MXXT A. 23°C, dry gas. We suppose that the test is run at a pressure of 1 atmosphere
		$2.67*10^{-16}$ [37]	25°C, 25 µm-thick film, 100% R.H.		
		$9.14*10^{-18}$ [16]	p684, Table A-IV. 35°C, 90% R.H.		

Cellophane	$3^{*}\ 10^{9}$ - $5^{*}10^{9}$ [23]	$8.15^{*}10^{-17}$ [16]	p684, Table A-IV. 38°C, 90% R.H.	$1.90^{*}\ 10^{-19}$ - $1.90^{*}10^{-18}$[23]	Goodfellow Cellophanem Rayophane Regenerated Cellulose Film
Poly(Vinyl Alcohol) (PVA)	$2.2^{*}10^{9}$ [38]	$1.29^{*}10^{-16}$ [25]	Table 1. 23°C, 85% R.H.	$1.10^{*}10^{-20}$ [25]	Table 1. 23°C, 50% or 0% R.H.
		$3.99^{*}10^{-18}$ [39]	Figure 7	$2.12^{*}10^{-18}$ [39]	Figure 6
		$1.74^{*}\ 10^{-17}$ - $8.71^{*}10^{-17}$ [16]	p684, Table A-IV. 40°C, 90% R.H.		
Ethylene Vinyl Alcohol (EVOH)	$1.08^{*}\ 10^{9}$ - $3.10^{*}10^{9}$ [23]	$1.31^{*}\ 10^{-18}$ - $1.13^{*}10^{-17}$ [23]	Overview of materials for Ethylene Vinyl Alcohol (EVOH)	$2.20^{*}\ 10^{-21}$ - $3.53^{*}10^{-20}$ [23]	Overview of materials for Ethylene Vinyl Alcohol (EVOH)
		$4.29^{*}\ 10^{-18}$ - $1.29^{*}10^{-17}$ [25]	Table 1. 23°C, 85% R.H.	$5.51^{*}\ 10^{-22}$ - $5.51^{*}10^{-21}$ [25]	Table 1. 23°C, 50% or 0% R.H.
		$3.90^{*}10^{-18}$ [27]	Ethylene Vinyl Alcohol (32% Ethylene). 25°C, 75% R.H. page 4320	$2.20^{*}10^{-21}$ [27]	Ethylene Vinyl Alcohol (32% Ethylene). 23°C, dry gas. We suppose that the test is run at a pressure of 1 atmosphere
				$5^{*}\ 10^{-22}$ - $6.65^{*}\ 10^{-20}$ [29-30]	Standard Temperature and Pressure conditions
Polyimide	$1.49^{*}\ 10^{9}$ - $3.1^{*}10^{9}$ [21, 40]	$7.21^{*}10^{-18}$ [40]	40°C, 100% R.H.		
		$5.37^{*}10^{-18}$ [41]	37,8°C, 90%RH and ASTM F1249	$9.15^{*}10^{-16}$ [17]	TMPA-6FDA Polyimide
Epoxy (unfilled)	$3.1^{*}10^{9}$ [21]	$1.78^{*}10^{-18}$ [41]	37,8°C, 90%RH and ASTM F1249		
Polylactic acid	$6^{*}\ 10^{8}$ - $8^{*}10^{8}$ [21]	$1.57^{*}10^{-17}$ [37]	25°C, 25 µm-thick film, 100% R.H.		
Parylene	$2.55^{*}10^{9}$ [42]	$1.11^{*}\ 10^{-19}$ - $1.19^{*}10^{-18}$ [42]	37°C, 90% R.H.	$1.52^{*}\ 10^{-18}$ - $6.84^{*}10^{-18}$ [42]	23°C. We suppose that 1 atm corresponds to a partial pressure of oxygen equal to 21000 Pa
Polytetrafluoroethylene (PTFE, alias Teflon)	$4.1^{*}10^{8}$ - $7.5^{*}10^{8}$ [21]	$1.42^{*}10^{-19}$ [43]	Test method: ASTM E-96-53T (vapor Pressure).	$8.33^{*}10^{-20}$ [43]	Test method: ASTM D-790-59 (at 1atm)
		$2.17^{*}10^{-19}$ [16]	p684, Table A-IV. 40°C, 90% R.H.		

Poly(4-methyl-1-pentene) (PMP)	$1.28*10^{9}$ [23]	$4.42*10^{-18}$ [23]	Honeywell PMP Polymethylpentene Film 100°F (37.8°C) / 100%RH; ASTM F1249	$2.03*10^{-16}$ [17]	
Polyester	$3.1*10^{9}$ - $4.36*10^{9}$ [23]	$2.47*10^{-20}$ - $2.47*10^{-19}$ [23]	37°C, 90% R.H.	$1.10*10^{-20}$ - $2.42*10^{-17}$ [23]	
				$1.12*10^{-18}$ [44]	Ambient pressure, 20°C
Polysulfone	$1.8*10^{9}$ - $3.2*10^{10}$ [23]			$9.00*10^{-18}$ [17]	
Inorganics					
Silica, SiO_x	$7.3*10^{10}$ [21]	$9.24*10^{-28}$ [45]	Tabke VI. 38°C, 90% R.H. for a 3 µm thick barrier		
		$3.70*10^{-24}$ [46]	Table 2. 40°C, 100% R.H. for a 40 nm thick barrier	$1.10*10^{-23}$ [46]	Table 2. 40°C, 90% R.H. for a 40 nm thick barrier
		$7.30*10^{-23}$ [47]	25°C, 100% R.H.	$8*10^{-27}$ [48]	<111> Silicon Wafer, at 1000°C. Diffusivity is given on Figure 5, and Oxygen solubility can be calculated from Figure 3, giving the oxygen concentration in Silicon.
		$4.7*10^{-27}$ [49]	65°C, 85% R.H., p 155 of the thesis. The diffusion coefficient must be lower than 10-15 cm2/s, and the solubility of water vapor in silica glass is about 0.001 gm/cc.atm. At 65°C, the vapor pressure of water is 25.02 kPa	$4.37*10^{-27}$ [50]	We use the formula for S and D in the abstract, for a temperature of 1600°C. We suppose that the partial pressure of oxygen is 21000 Pa
				$6.75*10^{-21}$ [51]	Vitreous Silica, at 900°C

				$5.00*10^{-24}$ [34]	Extrapolated from table 1 (PET / SiOx bilayers)
				$1.50*10^{-24}$ [34]	Extrapolated from table 1 (PET / SiOx bilayers)
				$4.9*10^{-23}$ [28]	Standard Temperature and Pressure conditions, from Figure 3
		$1.01*10^{-21}$ for one-side coating, and $1.28*10^{-22}$ for both-sides coating [36]	Table 2, 30°C. We use a molar volume of 24.5 mol/L for water vapor. 100% R.H. difference. Set-up: Permatran W600 from Modern Controls. The thickness of Silica ranges between 78 nm and 100 nm, we chose an average value of 89 nm for the calculations.	$1.40*10^{-22}$ for one-side coating, and $5.75*10^{-23}$ for both-sides coating [36]	Permeance measurements for oxygen were obtained using a temperature-controlled OxTran 2/20 from Modern Controls, Inc. Oxygen gradient across the film system was kept at a constant 1 atm, 100% oxygen concentration on the upstream side of the film vs 1 atm, 98% nitrogen/2% hydrogen carrier gas on the downstream side. Water vapor content on both sides of the test film was kept at 0% relative humidity. Data shown here are for 30°C.
		$2.25*10^{-24}$ - $1.50*10^{-22}$ [52]	Deposition on PET substrate, by PECVD. Thickness in the range [10 - 200] nm	$4.50*10^{-24}$ - $1.50*10^{-23}$ [52]	Deposition on PET substrate, by PECVD. Thickness in the range [10 - 200] nm
Silicon Nitride, SiN_x	$9.6*10^{10}$ - $3.2*10^{11}$ [21, 23]	$2.18*10^{-22}$ [53]	Figure 5, sputtering pressure 4 mTorr, 100nm thick film, at 40°C, 100% R.H.		
		$1.46*10^{-28}$ - $3.65*10^{-29}$ [54]	20°C, 50% R.H.		
				$6.00*10^{-24}$ [34]	Extrapolated from table 1 (PET / SiN bilayer)
		$1.13*10^{-24}$ - $7.50*10^{-24}$ [52]	Deposition on PET substrate, by PECVD. Thickness in the range [10 - 200] nm	$1.80*10^{-24}$ - $1.20*10^{-23}$ [52]	Deposition on PET substrate, by PECVD. Thickness in the range [10 - 200] nm

Al2O3/SiO2 bilayers		$7.60*10^{-27}$ - $1{,}10*10^{-24}$ [55]	Room temperature, 100% R.H.. Data extrapolated from Figure 5		
		$1.19*10^{-26}$ [56]	Table 2. 5nm Al2O3 / 60 nm SiOx		
Al2O3	$2.15*10^{11}$ - $4.13*10^{11}$ [24]	$9.43*10^{-27}$ [56]	Table 2. Deposited by ALD. 38°C		
		$7.30*10^{-25}$ [56]	Table 2. Deposited by PEALD. Room Temperature		
Al2O3/ZrO2	$3.10*10^{11}$ [23]	$1.76*10^{-27}$ [56]	Table 2. 70°C		
		$3.91*10^{-27}$ [57]	40 nm thick, 80°C, 80% R.H.		
TiO2	$2.3*10^{11}$ - $2.88*10^{11}$ [24]	$7.01*10^{-24}$ [56]	Table 2. Deposited by PEALD. Room Temperature		
Aluminum	$6.8*10^{10}$ [23]	$2.05*10^{-26}$ - $8.17*10^{-25}$ [58]	Figure 2. 38°C, 90% R.H.	$1.88*10^{-24}$ [34]	Extrapolated from table 1 (PET /Al bilayer)
			$8.19*10^{-24}$ - $1.57*10^{-23}$ [44]		20°C, ambient pressure of oxygen - this paper confirms that the permeability of sputtered Aluminum on Polyester is governed by defects density
Graphene	$1.0*10^{12}$ [59]	$3.42*10^{-30}$ [60]	Graphene monolayer on Surlyn substrate. 27°C, 90% R.H.	$1.12*10^{-30}$ - $1.79*10^{-28}$ [61]	Figure 8. 35 °C and 0% R.H., according to the specific ASTM Standard D 1434. Molar volume of Oxygen taken to be 22.4 L/mol
		$1.14*10^{-29}$ [60]	Graphene monolayer on PE substrate. 27°C, 90% R.H.		
		$9.12*10^{-28}$ [60]	Graphene monolayer on Saran substrate. 27°C, 90% R.H.		

Stiffness – Transmissibility trade-off for laminate and brick-mortar composites

Laminate. The laminate structure is made of a thick substrate and a thin film (Figure S1a). The thin film is stiffer but has a much lower permeability than the substrate. In steady state, the flux through each layer is equal. Using equation (1) and defining the transmissibility as T = P/h, we can derive the effective transmissibility of the laminate:

$$\frac{1}{T_{eff}} = \frac{1}{T_s} + \frac{1}{T_f} \tag{3}$$

Where T_s, T_f, and T_{eff} are respectively the permeability of the substrate, the film, and the laminate. When the laminate is stretched in the planar direction, both the film and the substrate share the load. The effective in-plane tensile stiffness E_{eff} of the laminate is:

$$(h_s + h_f)E_{eff} = h_s E_s + h_f E_f \tag{4}$$

Where E_s and E_f are the Young's moduli of the substrate and the film. h_s and h_f are the thicknesses of the substrate and the film. When the ratio h_f/h_s increases, the transmissibility of the laminate decreases while its stiffness increases (Figure S1b). Two quantitative examples are given: a plastic film on VHB and Silica (SiO_2) on VHB. For VHB, $P_s = 4\times10^{-17}$ $m^2.s^{-1}.Pa^{-1}$ and $E_s = 1$ MPa. For the plastic film, we choose numbers corresponding to high-density polyethylene (Table S1), with $P_f = 2\times10^{-19}$ $m^2.s^{-1}.Pa^{-1}$ and $E_f = 1$ GPa. For Silica, we choose $P_f = 1\times10^{-24}$ $m^2.s^{-1}.Pa^{-1}$ and $E_f = 73$ GPa. In case of Silica deposited on VHB, a decrease in transmissibility by three orders of magnitude compared to the bare substrate corresponds to an increase in stiffness by less than one order of magnitude. Even though the laminate is soft, it is not

stretchable because silica will crack at small strains. This solution does not allow low-transmissibility, soft and stretchable coatings.

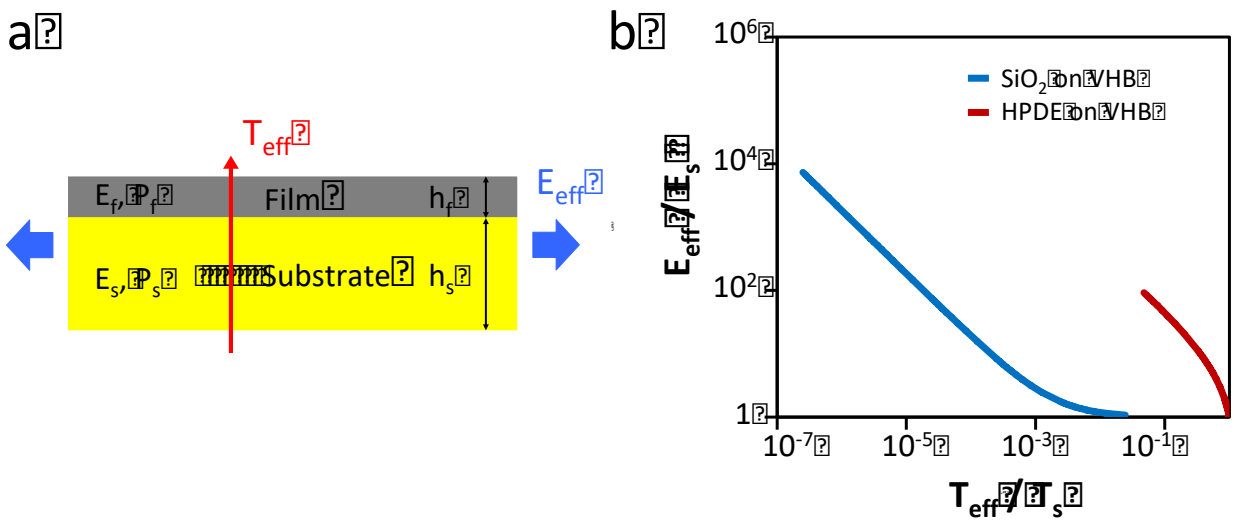

Figure S1. A low- transmissibility laminate means a stiff structure. **a,** A laminate structure is made of a stiff and thin film deposited on a thick soft substrate. **b**, Effective mechanical properties versus improvement in transmissibility for the laminate solution, based on equation 2 and 3. For a given material, there is a segment representing a continuum of thicknesses ratio h_f/h_s, ranging from 10^{-1} to 10^{-6}.

Brick-mortar Structure. The brick-mortar structure is made of a mortar (usually a polymer), and bricks (large-aspect ratio nanoparticles with very low permeability). Most of the diffusing molecules are avoiding the bricks. Thus, the diffusion path is increased, and the effective transmissibility of the brick-mortar is lower than the one of the bare mortar (Figure S2a). For bricks with a large aspect ratio (b<<2L) and an infinitely low permeability, we derived the effective transmissibility (equation 8), based on Nielsen's model.[62-64]. The effective permeability P_{eff} of a perfectly stacked brick-mortar structure (Figure S2a) is:

$$\frac{P_{eff}}{P_s} = \frac{1 - f}{1 + \frac{L}{2b} f} \tag{5}$$

where ϕ is the volume fraction of bricks and P_S is the permeability of the matrix. 2L is the length of a brick (Figure S2a).

ϕ can be expressed in function of the unit cell parameters:

$$f = \frac{8bL^2}{8bL^2 + 4hL^2} \tag{6}$$

We neglect here the volume of mortar between the flakes of the same layer, which is very small compared to the volume of mortar between two flakes of adjacent layers. Where L^2 drops out. Thus,

$$\frac{P_{eff}}{P_s} = \frac{1 - \frac{2b}{2b+h}}{1 + \frac{L}{2b+h}} \tag{7}$$

And the ratio of transmissibilities can be expressed:

$$\frac{T_{eff}}{T_S} = \frac{P_{eff}}{P_S} \frac{h}{h+b} = \frac{1 - \frac{2b}{2b+h}}{1 + \frac{L}{2b+h}} \frac{h}{h+b} \tag{8}$$

The brick-mortar structure has also been used widely in mechanics to explain toughening mechanisms in composites. Using the shear-lag model[65-66], we derived the effective tensile stiffness (equation 16) of the brick-mortar. Let E_b be the elastic modulus of the brick, G the shear modulus of the matrix. The matrix is an incompressible elastomer, so that the elastic modulus of the matrix is $E_s=3G$. τ (x) is the shear stress in the matrix, and σ_i is the normal stress in the brick i along the x direction (Figure S2a). Considering the force balance condition for the two bricks, we can get:

$$t(x) = b \frac{d\sigma_1(x)}{dx} = - b \frac{d\sigma_2(x)}{dx} \tag{9}$$

Because h is small, the matrix is undergoing a pure shear deformation. $\tau = G.\gamma$ where γ is the shear strain, and at small strains, $\gamma = [u_1-u_2]/h$, where u_i is the displacement of the brick i. Thus,

$$\frac{d\tau(x)}{dx} = \frac{G}{h}\left(\frac{du_1(x)}{dx} - \frac{du_2(x)}{dx}\right) = \frac{G}{E_b h}(\sigma_1(x) - \sigma_2(x)) \qquad (10)$$

Combining equation (8) and (9), we get the following boundary – value problem:

$$\begin{cases} \dfrac{d^2\sigma_1(x)}{d^2x} = \dfrac{G}{E_b hb}(\sigma_1(x) - \sigma_2(x)) \\ \dfrac{d^2\sigma_2(x)}{d^2x} = \dfrac{G}{E_b hb}(\sigma_2(x) - \sigma_1(x)) \end{cases} \qquad (11)$$

$$\begin{cases} s_1(0) = 0, s_1(L) = s_0 \\ s_2(0) = s_0, s_2(L) = 0 \end{cases}$$

Which has the solution:

$$s_1(x) = \frac{s_0}{\sinh\left(\frac{\lambda L}{2}\right)}\sinh\left(\frac{\lambda x}{2}\right)\cosh\left(\frac{\lambda (L - x)}{2}\right)$$

$$s_2(x) = s_1(L - x) = \frac{s_0}{\sinh\left(\frac{\lambda L}{2}\right)}\cosh\left(\frac{\lambda x}{2}\right)\sinh\left(\frac{\lambda (L - x)}{2}\right) \qquad (12)$$

$$\lambda = \sqrt{\frac{2G}{E_b hb}}$$

And we can express the shear stress as:

$$t(x) = \frac{s_0 b\lambda}{2\sinh\left(\frac{\lambda L}{2}\right)}\cosh\left(\lambda\left(x - \frac{L}{2}\right)\right) \qquad (13)$$

And the displacement field can be obtained by integration:

$$u_1(x) = \frac{\sigma_0}{2\lambda E_b}\left[\lambda x + (1+\cosh(\lambda x))\coth(\frac{\lambda L}{2}) - \sinh(\lambda x)\right]$$
$$u_2(x) = \frac{\sigma_0}{2\lambda E_b}\left[\lambda x + \sinh(\lambda x) + (1-\cosh(\lambda x))\coth(\frac{\lambda L}{2})\right] \quad (14)$$

Thus, the effective stress and the effective strain are:

$$\varepsilon_{eff} = \frac{u_1(L)}{L} = \frac{\sigma_0}{2\lambda E_b L}\left[\lambda L + 2\coth(\frac{\lambda L}{2})\right]$$
$$\sigma_{eff} = \sigma_0\left(\frac{b}{2b+h}\right) \quad (15)$$

The effective elastic modulus of the brick-mortar structure is,

$$E_{eff} = \frac{\sigma_{eff}}{\varepsilon_{eff}} = \frac{2E_b\lambda bL}{(2b+h)\left[\lambda L + 2\coth\left(\frac{\lambda L}{2}\right)\right]} \quad (16)$$

With $$\lambda = \sqrt{\frac{2G}{E_b hb}}$$

When the spacing h between bricks decreases, the transmissibility decreases and the stiffness increases (Figure S2b). We choose a matrix with an elastic modulus of 1 MPa, bricks with an elastic modulus of 73 GPa (SiO_2). The thickness of the bricks is set to 10 nm. Blue line is for L = 1 μm, while red line is for L = 10 μm. The thickness h between bricks is increasing when going to the left of a curve. A significant decrease in effective transmissibility implies again a huge increase in stiffness compared to the bare substrate. This solution enables to reduce the transmissibility without having to cast a defect-free thin film like in the case of the laminate. This approach is more scalable because it is less sensitive to defects (cracks, pinholes in the stiff material). In the limit of infinitely large bricks, the brick mortar just becomes a standard laminate. Thus, this solution cannot be as efficient as the laminate.

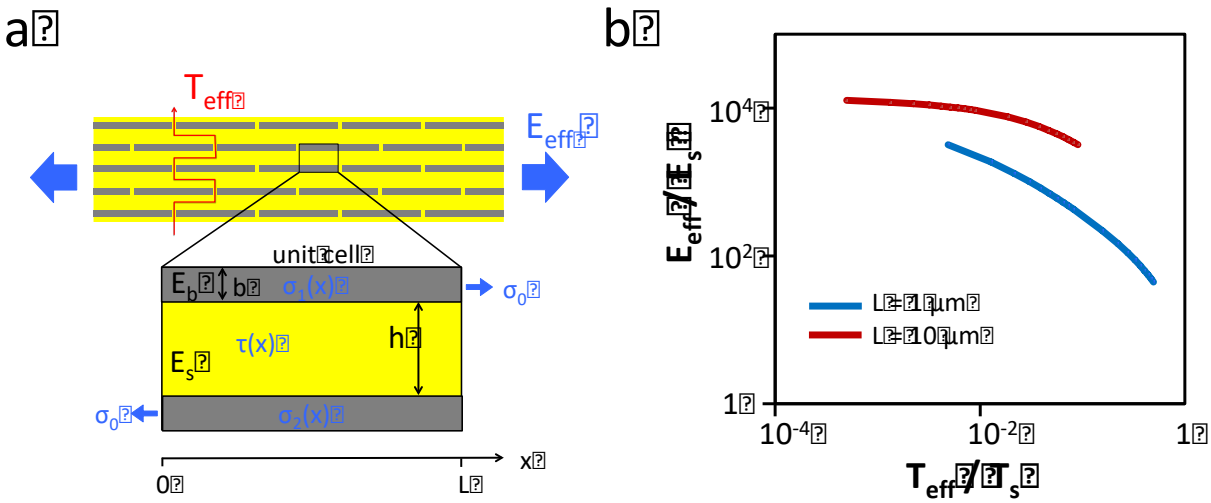

Figure S2. A low-transmissibility brick-mortar implies a stiff structure. **a**, The soft matrix (yellow) is undergoing pure shear deformation when the brick-mortar structure is under tension. **b**, Effective mechanical properties versus improvement in transmissibility for the brick-mortar solution. E_b is set to 73 GPa, E_s is 1 MPa, and b is 10 nm. Along a given curve, the spacing h between the bricks varies from 10 nm to 1 μm.

Analogy with the bending of an elastica

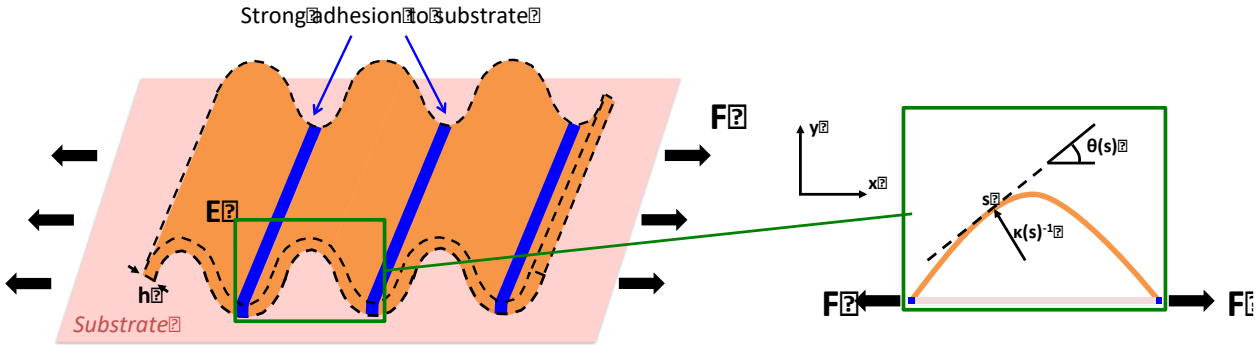

Figure S3. The geometry of deformation for a wavy film is analogous to the bending of an elastica.

Dimensional analysis. When the thin film is undergoing uniaxial bending, what happens in a cross-section containing the direction of the applied force is analogous to the bending of an elastica (Figure S3). The bending stiffness of the film is

$$D = \frac{1}{12}\frac{Eh^3}{(1-v)} \quad (17)$$

where ν is the Poisson's ratio, E is the elastic modulus of the material, and h the thickness of the film.

The force-displacement relation can be derived by dimensional analysis:

$$\frac{F}{w} = \frac{D}{L^2} f\left(\frac{\delta l}{L}\right) \quad (18)$$

where F is the in-plane force applied, w is the width of the film, L is the period of the wrinkles (Figure S3), and f is a dimensionless function of the effective tensile strain $\delta l/L$.

Force-elongation relation for the bending of an elastica. The boundary value problem of the elastica can be solved numerically. The elastica is a 1D inextensible line of material particle, which can sustain a bending moment.[67-71] We also note D the bending stiffness of the elastica. An elastica buckles under an axial force F. Let s be location of material particle (Figure S3), measured as the length long the elastica. In the current state, the material particle s moves of the location of the coordinates $x(s)$ and $y(s)$. Let the slope of the elastic be $q(s)$, and the curvature of the elastica be $k(s)$. D is the bending stiffness of the elastica. The governing equations are:

$$\frac{dk}{ds} = -\frac{F}{D}\sin q \quad (19.1)$$

$$\frac{dx}{ds} = \cos q \quad (19.2)$$

$$\frac{dy}{ds} = \sin q \quad (19.3)$$

$$\frac{dq}{ds} = k \quad (19.4)$$

Equation (19.1) is the balance of angular momentum, and equations (19.2), (19.3), and (19.4) are geometrical relations. When the elastica is straight, the length between the two ends is L. When the elastica bends, the length between the two ends shortens by δl. We set the boundary conditions to be:

$$x(0)=0,\quad y(0)=0,\quad k(0)=0, \qquad (20.1)$$

$$y(L)==0,\quad k(L)=0. \qquad (20.2)$$

A measure of stretchability is $\frac{\delta l}{L}$.

This system of PDE can be reduced to an ODE with two boundary conditions:

$$\frac{d^2q}{ds^2}=-\frac{F}{D}\sin q \qquad (21.1)$$

$$\frac{dq(0)}{ds}=0\ ,\ \frac{dq(L)}{ds}=0 \qquad (21.2)$$

We solve this boundary value problem using the shooting method on Mathematica (using the function NDSolve along with the Method "Shooting"). The coordinates of the material points in the deformed state are obtained by integration, using (19.2) and (19.3). The bifurcation diagram is plotted on Figure S4a. We plot the shape of the elastica for different values of the applied force on Figure S4b. $\frac{\delta l}{L}=x[1]-x[0]$ is the stretchability.

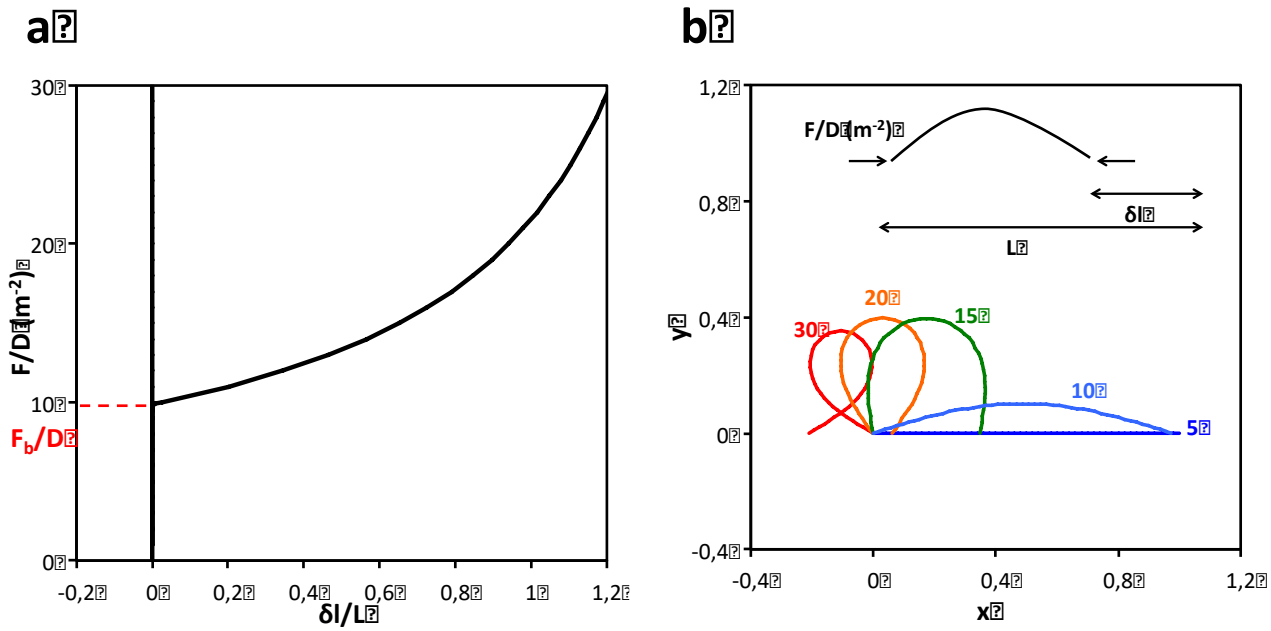

Figure S4. a, The bifurcation diagram shows that the elastica will buckle above a load F_b/D. **b,** The buckled elastica shortens more and more when the load increases. Thus, the stretchability $\frac{dl}{L}$ increases.

Below a critical load, the elastica remains flat. Above a critical load F_b (known as Euler's buckling load), the elastica can remain flat (unstable state), or buckle. Thanks to the bifurcation diagram, we can identify the dimensionless function f in equation (18). Right after buckling ($F>F_b$), we can interpolate linearly the force – strain relation as follow:

$$F - F_b = 5.56 \frac{D}{L^2} \frac{\delta l}{L} \qquad (22)$$

The interpolation coefficient is $R^2 > 0.999$ for a linear interpolation in the range $0 < \frac{dl}{L} < 0.2$.

In case of a thin film, the bending stiffness is given by equation (17). Equation (22) can be applied to a cross-section of the wavy film. The force F is becomes the force

per unit width F/w, and the bending stiffness of the elastica is replaced by the bending stiffness of the film:

$$\frac{F-F_b}{w} = \frac{5.56}{12(1-\nu)} \frac{Eh^3}{L^2} \frac{\delta l}{L} \qquad (23)$$

This relation has been derived for a compressive force and describes a purely elastic deformation. Thus, it still holds true for a tensile force when the film is already buckled.

Mechanical testing of polyethylene and aluminum wrinkles

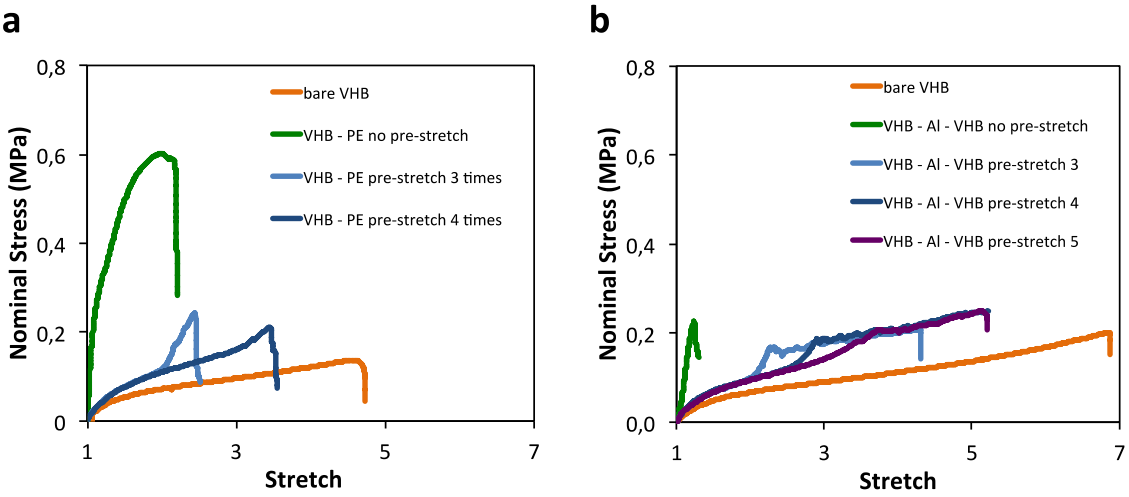

Figure S5. Uniaxially wrinkled laminates are soft and stretchable in uniaxial tension. **a**, Polyethylene (27 μm)/ VHB (500 μm) laminates with a pre-stretch of 0, 3, or 4 times. **b**, VHB (2 mm)/aluminum (26.5 μm)/VHB (2 mm) laminates with a pre-stretch of 0, 3, 4 or 5 times. The wrinkled laminates stiffen and break when the applied stretch overcomes the uniaxial pre-stretch.

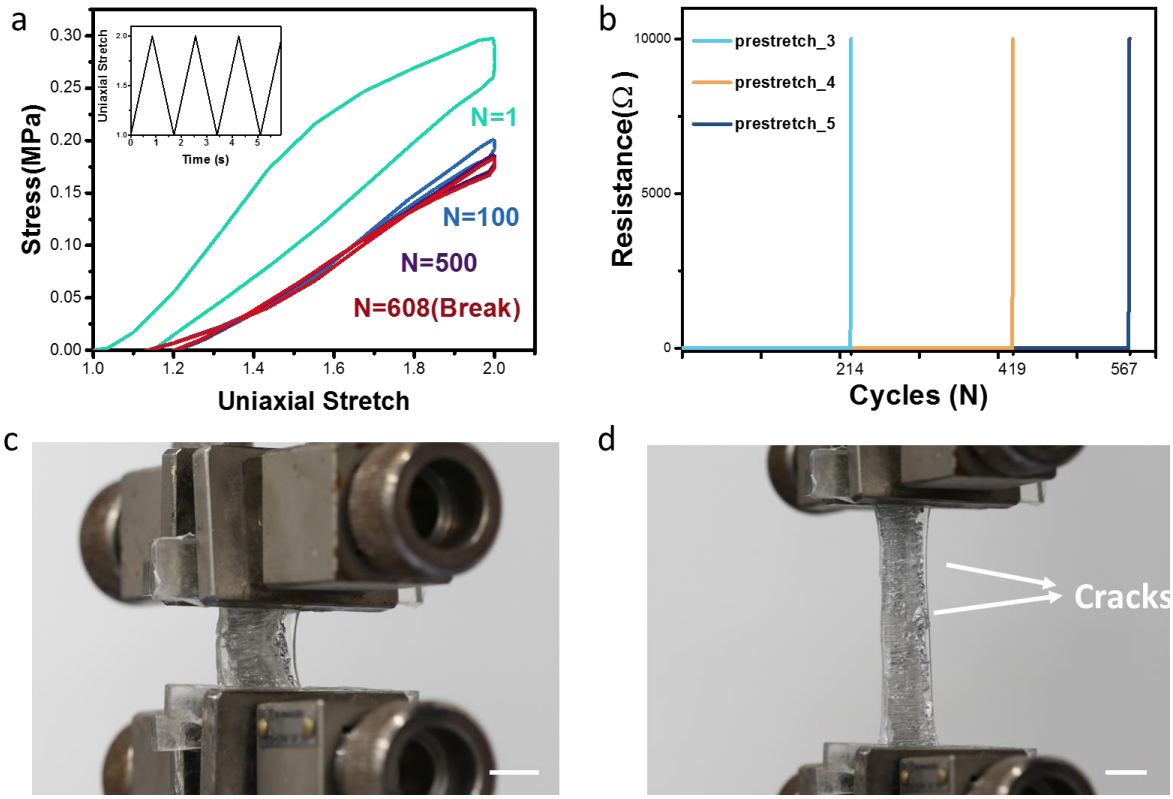

Figure S6. Fatigue test of VHB/aluminum/VHB in uniaxial tension. **a,** Nominal Stress-Strain curves (uniaxial pre-stretch of 5). The wrinkled laminate remains intact after 600 cycles. **b,** Resistance of the aluminum foil with the number of cycles. The resistance of metallic coating sharply increases from zero to infinite when it fails. When the pre-stretch is increased, the sample shows better fatigue resistance. **c,** Initial state of a sample with a pre-stretch of 4. **d,** After 413 cycles, the aluminum inside the sample breaks. Scale bars are 1 cm.

Model for the transmissibility of a wrinkled laminate

When we prepare a wrinkled laminate, we apply an in-plane pre-stretch λ_p to an elastomer, then we put a flat plastic film on top, and finally we release the pre-stretch. A residual in-plane stretch λ_r always remains, because of the elastic energy stored in the wrinkled plastic film (Figure S7). Since the elastomer is incompressible,

its thickness is reduced by a factor λ_r in the final state. We suppose that the area of plastic is not changed by the release of the pre-stretch. Thus, in the final state, the area of wrinkled plastic is larger than the area of elastomer, by a factor λ_p/λ_r.

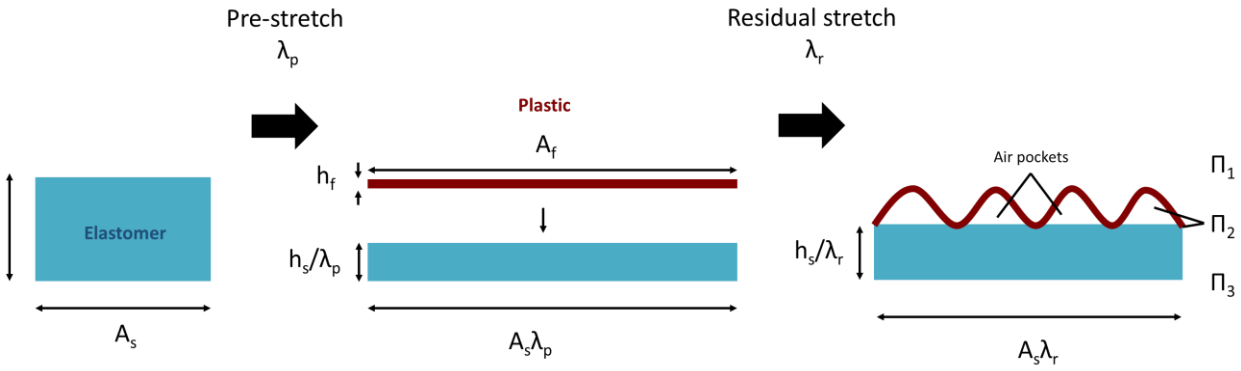

Figure S7. The area of wrinkled plastic is larger by a factor λ_p/λ_r. We suppose that the partial pressure of water vapor Π_2 film is the same everywhere between the elastomer substrate and the wrinkled plastic.

To determine the transmissibility of this structure, we suppose that the partial pressure of water vapor is the same at each point of the interface between the elastomer and the plastic. In Figure S7, it means that both the air pockets and the adhesion points between those have a partial pressure Π_2. In a steady-state, the total flux of water Q going through the wrinkled laminate is the same through each layer. According to equation (1) of the main text, we can write:

$$Q = P_f \frac{(\Pi_1 - \Pi_2)}{h_f} A_f = P_s \frac{(\Pi_2 - \Pi_3)}{h_s/\lambda_r} A_s \lambda_r \qquad (24)$$

Where the subscripts "f" and "s" respectively refer to the film and the substrate. P_i is the permeability, h_i is the initial thickness, and A the initial area of the layer "i". Π refers to the partial pressures of water, as indicated on Figure S5.

The effective transmissibility of the film T_{eff} is:

$$T_{eff} = \frac{Q}{A_s \lambda_r (\Pi_1 - \Pi_3)} \qquad (25)$$

Which we can rewrite using equation (22):

$$T_{eff} = \frac{1}{\frac{1}{\lambda_r}\frac{h_s}{P_s} + \frac{A_s \lambda_r}{A_f}\frac{h_f}{P_f}} \qquad (26)$$

According to the previous considerations, $A_s/A_f = \lambda_r/\lambda_p$. Thus,

$$T_{eff} = \frac{1}{\frac{1}{\lambda_r}\frac{h_s}{P_s} + \frac{\lambda_r^2}{\lambda_p}\frac{h_f}{P_f}} \qquad (27)$$

Which can be rewritten,

$$\frac{1}{T_{eff}} = \frac{1}{\lambda_r}\frac{1}{T_s} + \frac{\lambda_r^2}{\lambda_p}\frac{1}{T_f} \qquad (28)$$

With $T_s = \frac{P_s}{h_s}$ and $T_f = \frac{P_f}{h_f}$.

The propagation of the error in this model can be calculated as well. Assuming that the four experimental measurements T_s, T_s, λ_p, and λ_r are independent variables, the combined standard uncertainty[72] on T_{eff} is:

$$\sigma_{T_{eff}} = \sqrt{\left(\frac{\partial T_{eff}}{\partial T_s}\right)^2 \sigma_{T_s}^2 + \left(\frac{\partial T_{eff}}{\partial T_f}\right)^2 \sigma_{T_f}^2 + \left(\frac{\partial T_{eff}}{\partial \lambda_p}\right)^2 \sigma_{\lambda_p}^2 + \left(\frac{\partial T_{eff}}{\partial \lambda_r}\right)^2 \sigma_{\lambda_r}^2} \qquad (29)$$

Which can be rewritten explicitly,

$$\frac{\sigma_{T_{eff}}}{T_{eff}} = \sqrt{\left(\frac{T_{eff}}{\lambda_r T_s^2}\right)^2 \sigma_{T_s}^2 + \left(\frac{\lambda_r^2}{\lambda_p}\frac{T_{eff}}{T_f^2}\right)^2 \sigma_{T_f}^2 + \left(\frac{\lambda_r^2}{\lambda_p^2}\frac{T_{eff}}{T_f}\right)^2 \sigma_{\lambda_p}^2 + \left(\frac{2\lambda_r T_{eff}}{\lambda_p T_f} - \frac{T_{eff}}{\lambda_r^2 T_s}\right)^2 \sigma_{\lambda_r}^2} \qquad (30)$$

Where σ_i is the standard deviation or the typical error, on the measurement of parameter "i". The typical error on the stretches is $\sigma_{\lambda_p} = 0.1\lambda_p$ and $\sigma_{\lambda_r} = 0.1\lambda_r$. Experimental values and predictions for the water transmissibility of polyethylene/VHB and silica/PDMS laminates are compared on Figure S8, and errors bars on the predictions are calculated using equation (30).

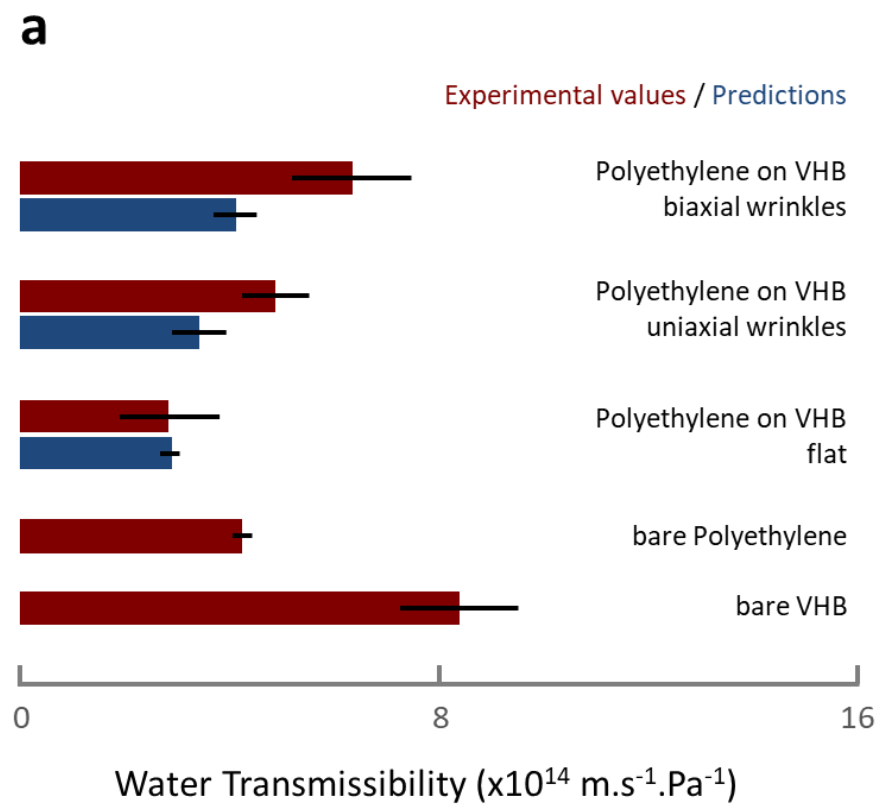
a
Experimental values / Predictions
Polyethylene on VHB
biaxial wrinkles
Polyethylene on VHB
uniaxial wrinkles
Polyethylene on VHB
flat
bare Polyethylene
bare VHB
0
8
16
Water Transmissibility (x10^14 m.s^-1.Pa^-1)

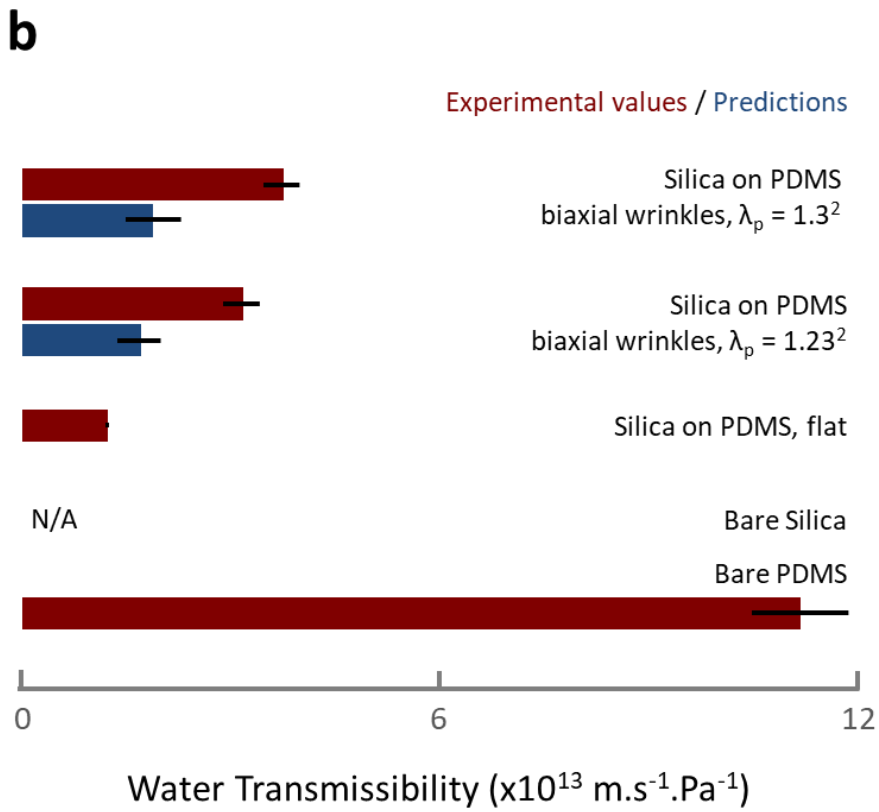
b
Experimental values / Predictions
Silica on PDMS
biaxial wrinkles, λp = 1.3^2
Silica on PDMS
biaxial wrinkles, λp = 1.23^2
Silica on PDMS, flat
N/A
Bare Silica
Bare PDMS
0
6
12
Water Transmissibility (x10^13 m.s^-1.Pa^-1)

Figure S8. The effective water transmissibility of wrinkled laminates is reduced compared to the bare substrate. a, Polyethylene (27 μm) on VHB (500 μm). The uniaxial pre-stretch of the VHB substrate is 4, and the residual uniaxial stretch 1.75. The biaxial pre-stretch of the VHB substrate is 10.6, and the residual biaxial stretch is 3.1. **b**, Silica (5 nm) on PDMS (200 μm). The biaxial pre-stretch of the PDMS substrate is 1.23x1.23 or 1.30x1.30. The residual biaxial stretch is negligible in this case. Absolute error bars on the experimental measurements represent one standard deviation on the transmissibility measurements. Absolute error bars on the predictions represent the standard uncertainty due to the scattering in the measurements of the transmissibility for the substrate and the stiff film, as well as the typical error on the measurements of the stretches.

Fatigue of wrinkled laminates in uniaxial tension

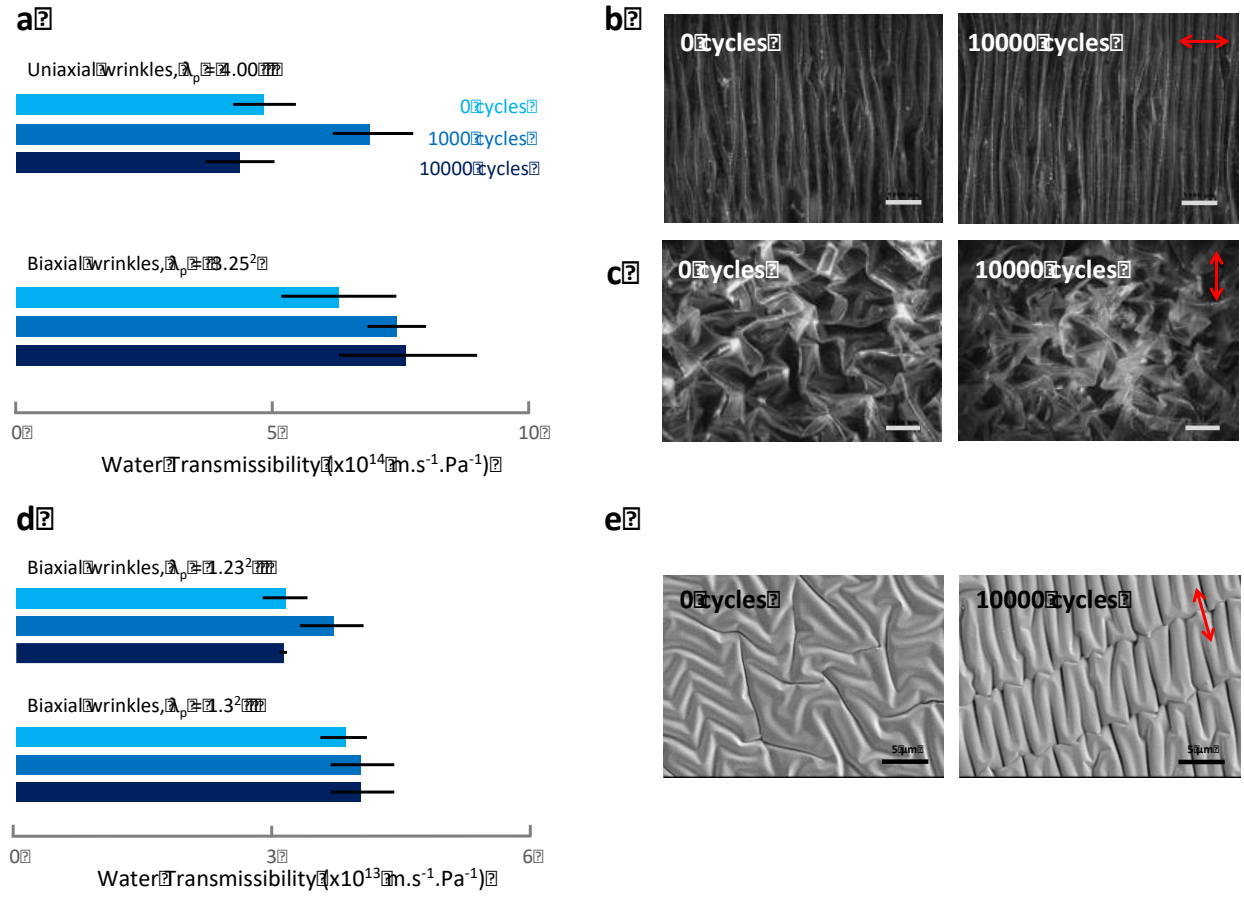

Figure S9. The transmissibility of polyethylene/VHB and silica/PDMS wrinkled laminates remains low after 10000 cycles of uniaxial tension. a, water transmissibility of polyethylene (27 μm)/VHB (500 μm) laminates only increases slightly with the number of cycles. The uniaxial strain applied to the uniaxially wrinkled laminate is 100%, and 50% for the biaxially wrinkled one. **b, c,** the morphology of the plastic wrinkles is not changed after 10000 cycles. The red arrow is the direction of the strain, and the scale bars are 1 millimeter. **d,** water transmissibility of silica (5 nm)/PDMS (200 μm) laminates only increases slightly with the number of cycles. The uniaxial strain applied are respectively 10% and 20% for the biaxially wrinkled laminates with λ_p = 1.23x1.23 and λ_p = 1.30x1.30. **e,** biaxial silica wrinkles are anisotropic after 10000 cycles of uniaxial tension. The red arrow is the direction of the strain, and the scale bars are 5 μm.

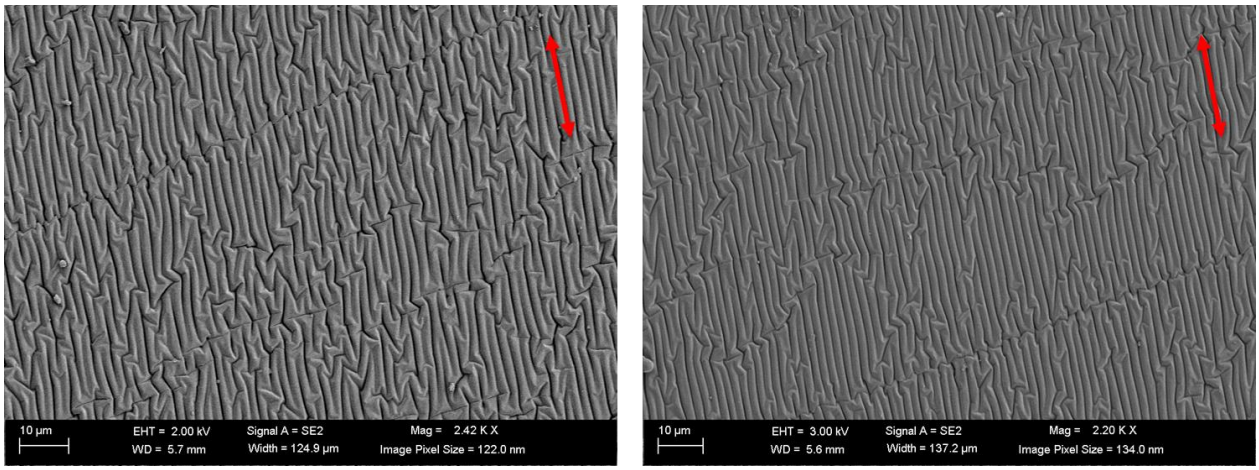

Figure S10. Anisotropy of silica wrinkles (5 nm) on a PDMS substrate (200 μm) after 10000 cycles of uniaxial tension. The pre-stretch applied was λ_p = 1.30x1.30, and the strain applied during the cyclic test is 20%. The red arrows indicate the direction of the strain. Spatially extended creases perpendicular to the stretching direction are formed.

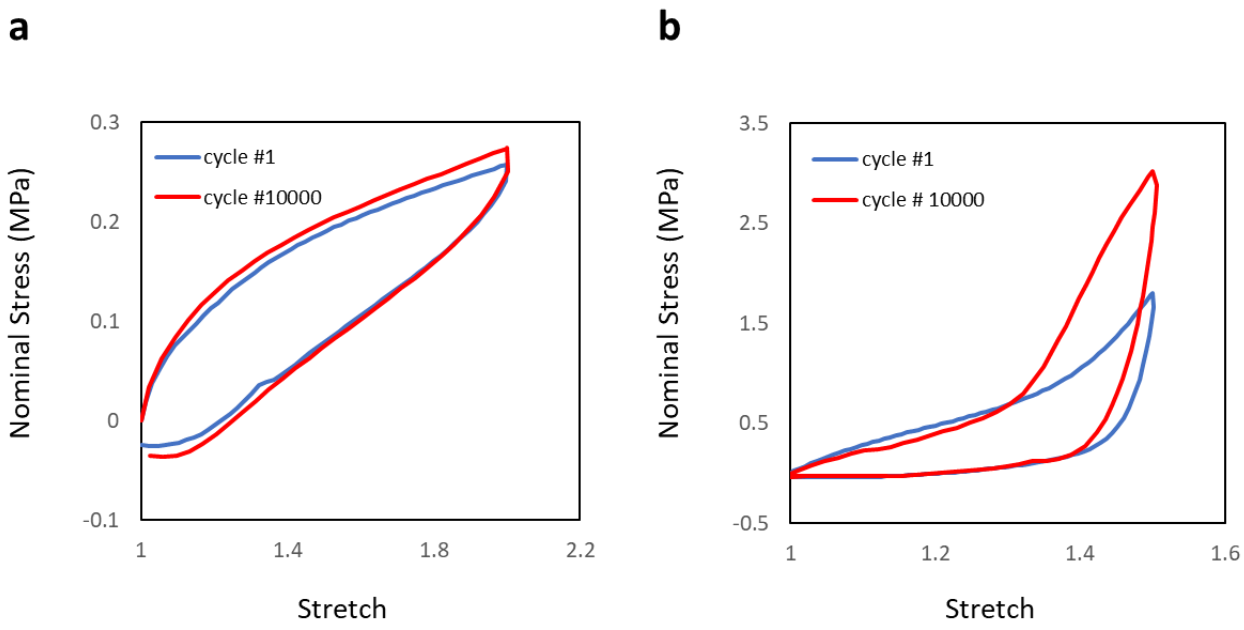

Figure S11. Stress – Stretch curves for polyethylene/VHB laminates with uniaxial wrinkles (a), and biaxial wrinkles (b), before and after 10000 cycles uniaxial tension. In case of biaxial wrinkles, we observe a stiffening at large stretches after 10000 cycles. We hypothesize that it is due to edge effects on the sample, where wrinkles became anisotropic.

Bibliography

1. Van Amerongen, G. J., The Permeability of Different Rubbers to Gases and Its Relation to Diffusivity and Solubility *Journal of Applied Physics* 1946, 17 (11), 972-985.
2. Anseth, K. S.; Bowman, C. N.; Brannon-Peppas, L., Mechanical Properties of Hydrogels and Their Experimental Determination *Biomaterials* 1996, (17), 1647-1657.
3. Lin, S.; Cao, C.; Wang, Q.; Gonzalez, M.; Dolbow, J. E.; Zhao, X., Design of Stiff, Tough and Stretchy Hydrogel Composites via Nanoscale Hybrid Crosslinking and Macroscale Fiber Reinforcement *Soft Matter* 2014, 10 (38), 7519-27.
4. Wise, D. L.; Houghton, G., The Diffusion Coefficient of Ten Slightly Soluble Gases in Water at 10-60°C *Chemical Engineering Science* 1966, 21, 999-1010.
5. Carpenter, J. H., New Measurement of Oxygen Solubility in Pure and Natural Water *Limnology and oceanography* 1966.
6. Tromans, D., Modeling Oxygen Solubility in Water and Electrolyte Solutions *Industrial & Engineering Chemistry Research* 2000, 39, 805-812.
7. Agache, P. G.; Monneur, C.; Leveque, J. L.; De Rigal, J., Mechanical Properties and Young's Modulus of Human Skin in Vivo *Archives of Dermatological Research* 1980, 269, 221-232.

8. Scheuplein, R. J., Handbook of Physiology, Reactions to Environmental Agents. 1977.
9. Ashby, M. F., Materials Selection in Mechanical Design fourth ed.; Elsevier 2011.
10. Department, U. o. C. E., Materials Databook 2003.
11. Helander, R. D.; Tolley, W. B. In Water Vapor Transmission Rate (WVTR) of Elastomeric Materials, Technology Vectors: 29th National SAMPE Symposium and Exhibition, MGM Grand Hotel, Reno, Nevada, April 3-5; MGM Grand Hotel, Reno, Nevada, 1984; pp 1373-1383.
12. Wolff, E. G., Introduction to the Dimensional Stability of Composite Materials 1 ed.; DEStech Publication 2004.
13. Van Amerongen, G. J., Influence of Structure of Elastomers on Their Permeability to Gases *Journal of Polymer Science* 1949, V (3), 307-332.
14. Le Floch, P.; Yao, X.; Liu, Q.; Wang, Z.; Nian, G.; Sun, Y.; Jia, L.; Suo, Z., Wearable and Washable Conductors for Active Textiles *ACS Appl Mater Interfaces* 2017, 9 (30), 25542-25552.
15. Iyengar, Y., Relation of Water Vapor Permeability of Elastomers to Molecular Structure *Polymer Letters* 1965, 3, 663-669.
16. Rogers, C. E., Permeability and Chemical Resistance. In Engineering Design for Plastics, Baer, E., Ed. Van Nostrand-Reinhold: Princeton, 1964.
17. Robeson, L. M., Polymer Membranes for Gas Separation *Current Opinion in Solid State and Materials Science* 1999, 4, 549-552.
18. McKeen, L. W., Permeability Properties of Plastics and Elastomers Third ed.; Matthew Deans Elsevier, 2012.
19. Illinger, J. L.; Schneider, N. S.; Karasz, F. E., Water Vapor Transport in Hydrophilic Polyurethanes. In Permeability of Plastic Films and Coatings, 1974; p 183–196.
20. 3M, VHB Tape Speciality Tapes 3M, Ed. 2014.
21. Matbase 2018.
22. Chemours, Viton A-401C Fluoroelastomers 2016.
23. Matweb 2018.
24. AZoM (online database) https://www.azom.com/ (accessed March 17th).
25. Lange, J.; Wyser, Y., Recent Innovations in Barrier Technologies for Plastic Packaging - a Review *Packag. Technol. Sci.* 2003, 16, 149-158.
26. Kamal, M. R.; Jinnah, I. A.; Utracki, L. A., Permeability of Oxygen and Water Vapor Through Polyethylene/Polyamide Films *Polymer Engineering & Science* 1984, 24 (17), 1337-1347.
27. Caballero, B.; Trugo, L.; Finglas, P. M., Encyclopedia of Food Sciences and Nutrition Second ed.; Academic Press 2003.
28. Leterrier, Y., Durability of Nanosized Oxygen-Barrier Coatings on Polymers *Progress in Materials Sciences* 2003, 48, 1-55.
29. Ryder, L., OXYGEN-BARRIER CONTAINERS-THEIR DESIGN AND COST *PLASTICS ENGINEERING* 1984, 40 (5), 41-48.
30. Brandrup, J.; Immergut, E. H.; Grulke, E. A.; Abe, A.; Bloch, D. R., Polymer Handbook Wiley New York etc 1989; Vol. 7.
31. Hernandez, R. J., Effect of Water Vapor on the Transport Properties of Oxygen through Polyamide Packaging Materials. In Water in Foods, Pergamon: Amsterdam, 1994; pp 495-507.
32. Miller, K. S.; Krochta, J. M., Oxygen and Aroma Barrier Properties of Edible Films: A Review *Trends in Food Science & Technology* 1997, 8 (7), 228-237.

33. Massey, L. K., Permeability Properties of Plastics and Elastomers Plastics Design Library / William Andrew Publishing 2003.
34. Chatham, H., Oxygen Diffusion Barrier Properties of Transparent Oxide Coatings on Polymeric Substrates *Surface and Coatings Technology* 1994, (78), 1-9.
35. Slee, J. A.; Orchard, G. A. J.; Bower, D. I.; Ward, I. M., The Transport of Oxygen through Oriented Poly(ethylene terephthalate) *Journal of Polymer Science Part B: Polymer Physics* 1989, 27 (1), 71-83.
36. Tropsha, Y. G. H., N. G., Activated Rate Theory Treatment of Oxygen and Water Transport through Silicon Oxide/ Poly(ethylene terephthalate) Composite Barrier Structures *J. Phys. Chem. B* 1997, 101, 2259-2266.
37. Shorgen, R., Water Vapor Permeability of Biodegradable Polymers *Journal of Environmental Polymer Degradation* 1997, 5 (2), 91-95.
38. Peijs, T.; Van Vught, R.; Govaert, L., Mechanical Properties of Poly(vinyl Alcohol) Fibres and Composites *Composites* 1995, 26 (2), 83-90.
39. Huang, H.-D.; Ren, P.-G.; Chen, J.; Zhang, W.-Q.; Ji, X.; Li, Z.-M., High Barrier Graphene Oxide Nanosheet/poly(vinyl alcohol) Nanocomposite Films *Journal of Membrane Science* 2012, 409-410, 156-163.
40. Tsai, M.-H.; Tseng, I. H.; Liao, Y.-F.; Chiang, J.-C., Transparent Polyimide Nanocomposites with Improved Moisture Barrier using Graphene *Polymer International* 2013, 62 (9), 1302-1309.
41. Jung, S.-Y.; Paik, K.-W., Effects of Alignment of Graphene Flakes on Water Permeability of Graphene-epoxy Composite Film In Electronic Components & Technology Conference, IEEE 64th, IEEE: Orlando, FL, USA, 2014.
42. TECH, P., Parylene Properties.
43. APG, Permeability of Teflon FEP Resins.
44. Jamieson, E. H. H.; Windle, A. H., Structure and Oxygen-Barrier Properties of Metallized Polymer Film *Journal of Materials Science* 1983, 18, 64 - 80.
45. Visweswaran, B.; Mandlik, P.; Mohan, S. H.; Silvernail, J. A.; Ma, R.; Sturm, J. C.; Wagner, S., Diffusion of Water into Permeation Barrier Layers *Journal of Vacuum Science & Technology A: Vacuum, Surfaces, and Films* 2015, 33 (3), 031513.
46. Hanada, T.; Negishi, T.; Shiroishi, I.; Shiro, T., Plastic Substrate with Gas Barrier Layer and Transparent Conductive Oxide Thin fFlm for Flexible Displays *Thin Solid Films* 2010, 518 (11), 3089-3092.
47. Wuu, D. S.; Lo, W. C.; Chiang, C. C.; Lin, H. B.; Chang, L. S.; Horng, R. H.; Huang, C. L.; Gao, Y. J., Plasma-Deposited Silicon Oxide Barrier Films on Polyethersulfone Substrates: Temperature and Thickness Effects *Surface and Coatings Technology* 2005, 197 (2-3), 253-259.
48. Itoh, Y.; Tadashi, N., Solubility and Diffusion Coefficient of Oxygen in Silicon *Japanese Journal of Applied Physics* 1985, 24 (3), 279-284.
49. Mandlik, P., A Novel Hybrid Inorganic-Organic Single Layer Barrier for Organic Light-Emitting Diodes Princeton University 2009.
50. Mikkelsen, J. R., The Diffusivity and Solubility of Oxygen in SIlicon *Mat. Res. Soc. Symp. Proc.* 1985, 59, 19-30.
51. Norton, F. J., Permeation of Gaseous Oxygen through Vitreous Silica *Nature* 1961, 4789, 701.
52. Czeremuszkin, G.; Klemberg-Sapieha, J. E.; Wertheimer, M. R., Transparent Barrier Coatings on Polyethylene Terephthalate by Single- and Dual-Frequency Plasma-Enhanced Chemical Vapor Deposition *J. Vac. Sci. Technol. A* 1998, 16 (6), 3190-3198.

53. Tsai, M.-H.; Wang, H.-Y.; Lu, H.-T.; Tseng, I.-H.; Lu, H.-H.; Huang, S.-L.; Yeh, J.-M., Properties of Polyimide/Al2O3 and Si3Ni4 Deposited Thin Films *Thin Solid Films* 2011, (519), 4969-4973.
54. Andringa, A. M.; Perrotta, A.; de Peuter, K.; Knoops, H. C.; Kessels, W. M.; Creatore, M., Low-Temperature Plasma-Assisted Atomic Layer Deposition of Silicon Nitride Moisture Permeation Barrier Layers *ACS Appl Mater Interfaces* 2015, 7 (40), 22525-22532.
55. Dameron, A. A.; Davidson, D. D.; Burton, B. B.; Carcia, P. F.; McLean, R. S.; George, S. M., Gas Diffusion Barriers on Polymers Using Multilayers Fabricated by Al2O3 and Rapid SiO2 Atomic Layer Deposition *J. Phys. Chem. C* 2008, (112), 4573-4580.
56. Park, J.-S.; Chae, H.; Chung, H. K.; Lee, S. I., Thin Film Encapsulation for Flexible AM-OLED: a Review *Semiconductor Science and Technology* 2011, 26 (3), 034001.
57. Meyer, J.; Schmidt, H.; Kowalsky, W.; Riedl, T.; Kahn, A., The Origin of Low Water Vapor Transmission Rates through Al2O3/ZrO2 Nanolaminates Gas-Diffusion Barriers grown by Atomic Layer Deposition *Applied Physics Letters* 2010, 96 (24), 117.
58. Dollinger, F.; Nehm, F.; Müller-Meskamp, L.; Leo, K., Laminated Aluminum Thin-Films as Low-Cost Opaque Moisture uUtra-Barriers for Flexible Organic Electronic Devices *Organic Electronics* 2017, 46, 242-246.
59. Lee, C.; Wei, X.; Kysar, J. W.; Hone, J., Measurement of the Elastic Properties and Intrinsic Strength of Monolayer Graphene *Science* 2008, 321 (5887), 385-388.
60. Seethamraju, S.; Kumar, S.; B, K. B.; Madras, G.; Raghavan, S.; Ramamurthy, P. C., Million-Fold Decrease in Polymer Moisture Permeability by a Graphene Monolayer *ACS Nano* 2016, 10 (7), 6501-6509.
61. Pierleoni, D.; Xia, Z. Y.; Christian, M.; Ligi, S.; Minelli, M.; Morandi, V.; Doghieri, F.; Palermo, V., Graphene-Based Coatings on Polymer Films for Gas Barrier Applications *Carbon* 2016, 96, 503-512.
62. Nielsen, L. E., Models for the Permeability of Filled Polymer Systems *Journal of Macromolecular Science: Part A - Chemistry* 1967, 1 (5), 929-942.
63. Bharadwaj, R. K., Modeling the Barrier Properties of Polymer-Layered Silicate Nanocomposites *Macromolecules* 2001, 34, 9189-9192.
64. Cui, Y.; Kundalwal, S. I.; Kumar, S., Gas Barrier Performance of Graphene/Polymer Nanocomposites *Carbon* 2016, 98, 313-333.
65. Launey, M. E.; Ritchie, R. O., On the Fracture Toughness of Advanced Materials *Advanced Materials* 2009, 21 (20), 2103-2110.
66. Wei, X.; Naraghi, M.; Espinosa, H. D., Optimal Length Scales Emerging from Shear Load Transfer in Natural Materials: Application to Carbon-Based Nanocomposite Design *ACS Nano* 2012, 6 (3), 2333-2344.
67. Euler, L., Methodus Inveniendi Lineas Curvas Maximi Minimive Proprietate Gaudentes Sive Solutio Problematis Isoperimetrici Latissimo Sensu Accepti 1744.
68. Love, A. E. H., A Treatise on The Mathematical Theory of Elastivity Cambridge University Press 1892.
69. Antman, S. S., Nonlinear Problems of Elasticity Second ed.; Springer 2005; Vol. 107.
70. Pacheco, M. E. P., E., The Elastic Rod *Revista mexicana de física E* 2007, 53 (2), 186-190.
71. Audoly, B. P., Y., Elasticity and Geometry Oxford University Press 2010.
72. JCGM, Evaluation of Measurement Data — Guide to the Expression of Uncertainty in Measurement 2008.